Title: Morphological adaptations of 3.22 Ga-old tufted microbial mats to Archean coastal habitats (Moodies Group, Barberton Greenstone Belt, South Africa)

Author: Martin Homann Christoph Heubeck Alessandro Airo Michael M. Tice

PII: S0301-9268(15)00130-8
DOI: http://dx.doi.org/doi:10.1016/j.precamres.2015.04.018
Reference: PRECAM 4247

To appear in: *Precambrian Research*

Received date: 23-1-2015
Revised date: 1-4-2015
Accepted date: 12-4-2015

Please cite this article as: <doi>http://dx.doi.org/10.1016/j.precamres.2015.04.018</doi>

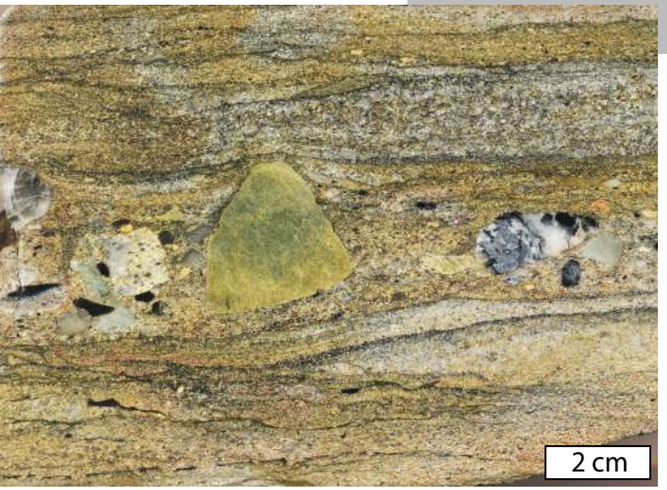

Coastal floodplain

- planar mats

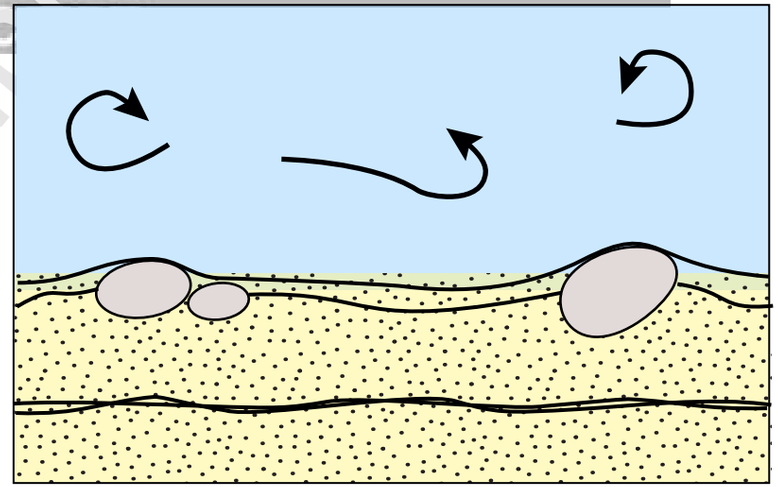

Intertidal

- wavy-crinkly mats with domes

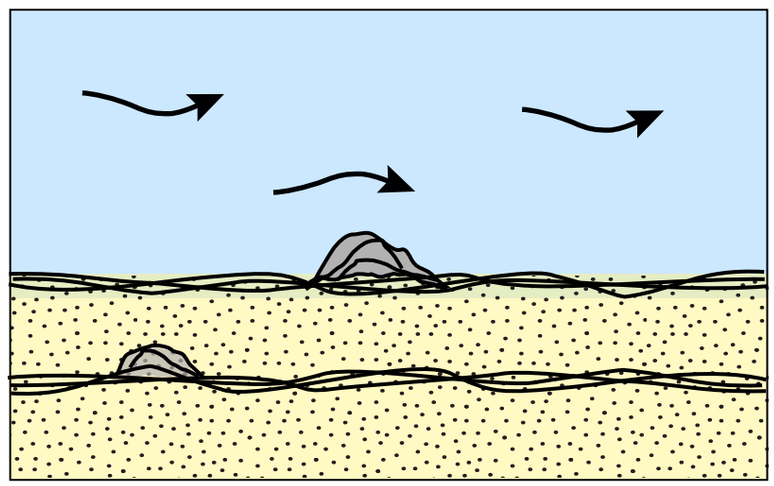

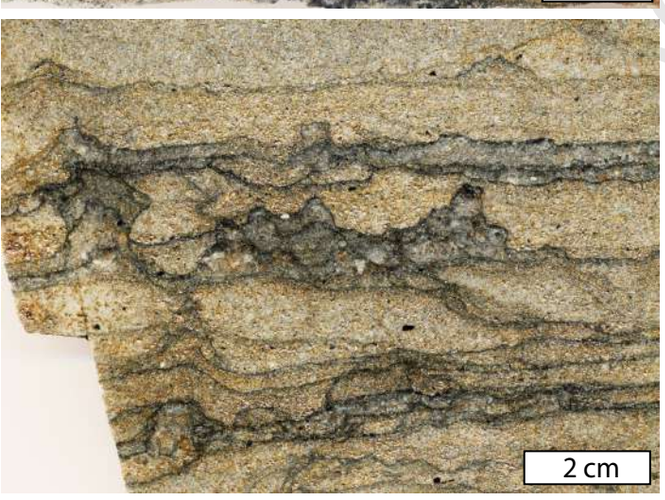

Upper inter- to supratidal

- tufted mats

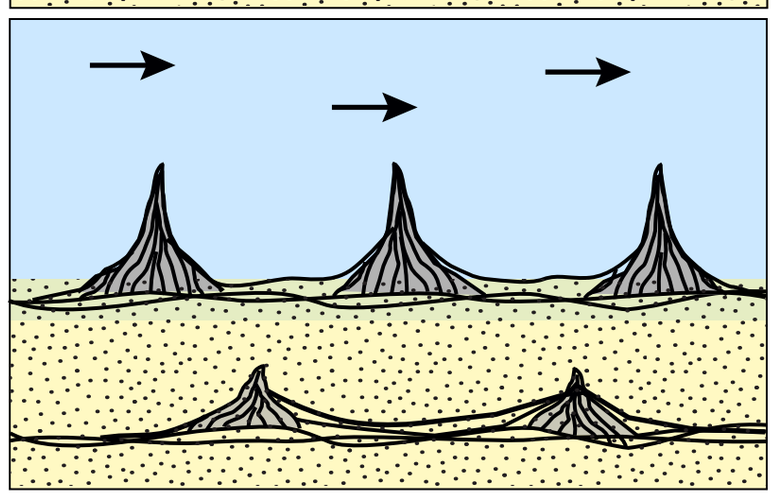

Morphological adaptations of 3.22 Ga-old tufted microbial mats to Archean coastal habitats (Moodies Group, Barberton Greenstone Belt, South Africa)

Martin Homann[a, *], Christoph Heubeck[b], Alessandro Airo[a], Michael M. Tice[c]

[a] Institut für Geologische Wissenschaften, Freie Universität Berlin, Malteserstr. 74-100, 12249 Berlin, Germany

[b] Institut für Geowissenschaften, Friedrich-Schiller-Universität Jena, Burgweg 11, 07749 Jena, Germany

[c] Department of Geology & Geophysics, Texas A&M University, College Station, Texas 77843, USA

[*]Corresponding author.

E-mail addresses: martin.homann@fu-berlin.de (M. Homann), christoph.heubeck@uni-jena.de (C. Heubeck), aairo@fu-berlin.de (A. Airo), mtice@geos.tamu.edu (M. Tice)

Abstract

Microbial life was well established and widespread by the Paleoarchean; however, the degree of evolutionary advancement such as microbial motility, intra- and inter-species interactions, phototropism, or oxygenic photosynthesis by that time remains highly debated. The 3.22 Ga Moodies Group in the Barberton Greenstone Belt (BGB, South Africa) are Earth's oldest well-preserved siliciclastic tidal deposits.They exhibit a unique assemblage of microbial mats, providing an excellent opportunity to decipher the morphological adaptations of microbial communities to different paleoenvironmental settings. The fossil mats are preserved as kerogenous laminations (0.5 to 1 mm thick) that can be traced laterally for ~15 km in a ~1000 m-thick succession of fine- to coarse-grained tidal sandstones and conglomerates. We here present a detailed stratigraphic and depositional facies analysis, documenting the association of the three principal mat morphotypes with specific environmental settings: (1) planar-type in coastal floodplain, (2) wavy-type in intertidal, and (3) tufted-type in upper inter- to supratidal facies. All mat types indicate a flourishing phototrophic biota; moreover, the tufted morphology suggests an intricate level of coordinated growth commonly known from cyanobacterial mats in modern environments.

1. Introduction

The study of the diversity and setting of early Archean ecosystems is essential for unraveling the phyolgenetic tree of life and the onset of oxygenic photosynthesis, the principal source of free oxygen in the atmosphere. Although the atmospheric oxygen concentration first rose globally and permanently during the 'Great Oxidation Event' (GOE), 2.5 - 2.3 Ga ago, several recent geochemical studies suggest a prolonged and dynamic transition from anoxic conditions, starting 3 Ga ago or even earlier (Holland, 2002, 2006; Anbar et al., 2007; Buick, 2008; Farquhar et al., 2011; Crowe et al., 2013; Lyons et al., 2014; Mukhopadhyay et al., 2014; Planavsky et al., 2014; Lalonde and Konhauser, 2015).

Studies aiming to investigate the structure and diversity of early microbial communities are essentially restricted to two locations worldwide in which sedimentary rocks have escaped regional high-grade metamorphism and penetrative deformation: the Pilbara Craton of Western Australia and the Barberton Greenstone Belt (BGB) of the Kaapvaal Craton of southern Africa. In the strata of the BGB, a variety of microbial traces are preserved, e.g., carbonaceous chert containing filamentous, coccoidal and spindle-shaped microfossils (Walsh and Lowe, 1985, 1999; Walsh, 1992; Westall et al., 2006), planar microbial mats (Tice et al., 2004; Tice and Lowe, 2006; Tice, 2009), pseudocolumnar, stromatolite-like structures (Byerly et al., 1986; Walsh and Westall, 2003 and references therein), and organic-walled, spheroidal microfossils (Javaux et al., 2010). Moreover, the BGB includes the world's oldest known regionally mappable record of microbial mats in a siliciclastic tidal setting, exposed in the 3.22 Ga, and remarkably well-preserved Moodies Group (Noffke et al., 2006; Heubeck, 2009; Gamper et al., 2012).

Initially, the macroscopic laminations described here were interpreted as shale partings in horizontally bedded sandstones (Visser, 1956; Eriksson, 1977); however, Heubeck and Lowe (1994) noted that the laminae were anastomosing in cross-section and exhibited mushroom-

shaped protrusions. Subsequently, Noffke et al. (2006), Heubeck (2009), and Gamper et al. (2012) established their biogenicity, based on carbonaceous composition, sedimentary environment, negative $\delta^{13}C$ values (-20.1 ‰ to -22.5 ‰), and specific local textures such as eroded microbial mat fragments and fluid-escape structures. We here present the first detailed characterization of the paleoenvironmental context of the Moodies mats, and discuss the environmental adaptation of the mats in comparison with modern microbial ecosystems.

2. Regional Geology

The Barberton Greenstone Belt (3.57 to ca. 3.22 Ga) of South Africa and Swaziland is located at the eastern margin of the Kaapvaal Craton (Fig. 1) and represents one of world's oldest Archean greenstone belts. The greenstone belt fill (the Barberton Supergroup, formerly Swaziland Supergroup) is subdivided into (1) the ~8 - 10 km thick, ca. 3.57 - 3.30 Ga volcanic-dominated Onverwacht Group (Viljoen and Viljoen, 1969; Anhaeusser, 1976; Lowe and Byerly, 2007; De Wit et al., 2011); (2) the up to 3 km thick, ca. 3.55 - 3.25 Ga Fig Tree Group, which includes mostly shale, banded iron-formation (BIF), and volcaniclastic sediments (Heinrichs and Reimer,1977; Condie, 1997; Lowe and Byerly, 1999; Hofmann, 2005); and (3) the up to 3.7 km thick, coarse silicilastic Moodies Group (Eriksson, 1977; Heubeck and Lowe, 1994a, 1994b, 1999). All BGB strata experienced several phases of major deformation during which they were extensively folded, faulted and altered (De Ronde and De Wit, 1994; Lowe and Byerly, 1999). A major fault system, the Inyoka Fault, transects the greenstone belt approximately medially. The dominant large-scale orogeny of the BGB took place contemporaneously with deposition of the Moodies Group at 3.225 - 3.215 Ma (Lamb and Paris, 1988; Heubeck et al., 2013).

3. The Moodies Group

Strata of the Moodies Group are laterally traceable and can be subdivided stratigraphically, allowing the identification of distinct facies and their transitions (Hall, 1918; Visser, 1956; Anhaeusser, 1976; Eriksson, 1977, 1978, 1979, 1980; Heubeck and Lowe, 1994a, 1999, 1994b; Eriksson and Simpson, 2000; Eriksson et al., 2006; Heubeck, 2009; Simpson et al., 2012). Moodies Group strata north of the Inyoka Fault are preserved in several, commonly northward-overturned synclines that are tectonically separated by major faults (Fig.1). Strata there are dominated by fine- to coarse-grained, quartz-rich sandstones that are locally interbedded with conglomerates and which were deposited in alluvial, fluvial, possibly aeolian, deltaic, tidal, and subtidal paleoenvironments (Anhaeusser, 1976; Eriksson, 1979, 1977; Heubeck and Lowe, 1999, 1994a; Eriksson and Simpson, 2000; Eriksson et al., 2006; Simpson et al., 2012). Minor components include shales, siltstones, BIF, thin tuffs, and a single basaltic lava (Bontognali et al., 2013; Heubeck et al., 2013). Moodies Group strata south of the Inyoka Fault are dominated by coarse-grained, gravelly sandstones that lack feldspar and marker units and have not been correlated with the strata north of the fault (Heubeck and Lowe, 1994a). The Moodies Group north of the Inyoka Fault was subdivided in several informal lithostratigraphic members and in three formally defined formations (Joe's Luck, Clutha, and Baviaanskop) by Visser (1956) and Anhaeusser (1976), respectively; Eriksson (1977) suggested an alternative subdivision in five fining-upward sequences (MD1 through MD5). Petrofacies trends in sandstone composition in the lower Moodies Group

were interpreted by Heubeck and Lowe (1994a) as indicative of an extensional setting, while the architecture and composition of the upper Moodies Group inidcated a response to syndepositional shortening along the northern margin of the greenstone belt and incipient basin uplift. The best-preserved and strain-free Moodies sandstones are silicified and occur in the interior of the central BGB, distant from major fault zones, BGB-marginal strain, and fold hinges. Based on isotopic resetting in barites and carbonates, the regional heating of the BGB was estimated to have reached a minimum temperature of ~200°C (De Ronde et al., 1991; Toulkeridis et al., 1998; Tice et al., 2004). The age of the Moodies Group is constrained by stratiform dacitic tuff beds and felsic dikes radiating from the Kaap Valley Tonalite (KVT) that crosscut beds of the Moodies Hills Block and Eureka Syncline along the northern margin of the BGB (Layer et al., 1996; Heubeck et al., 2013). Depositional ages of the volcanic beds throughout the Moodies Group, obtained through single-zircon U-Pb dating, indicate that deposition began ~3223 ± 1 Ma and had ended by ~3219 ± 9 Ma (De Ronde and Kamo, 2000; Heubeck et al., 2013). Consequently, the >3 km thick Moodies succession was deposited and deformed within <1 - 14 Ma and with that represents a unique, very-high-resolution archive of Archean surface and sedimentation processes, comparable in spatial and temporal resolution to many Quaternary sections.

One of the most intriguing features of Moodies sandstones is the occurrence of locally abundant, macroscopically visible, microbial mats and associated structures, preserved in exquisite detail, which are the focus of this work. Mapping and regional field studies demonstrate that these are preserved best in the overturned limb of the Saddleback Syncline in the central BGB in a ca. 3 km-thick succession of subvertically dipping, laterally continuous and unfaulted strata (Figs. 1 and 2). For the current study, we investigated strata of the lower section of this succession, which are equivalent to units MdB and MdQ1 of

Anhaeusser (1976) and to unit MD1 and MD3 of (Eriksson, 1977); they reach approximately 1350 m thick (Fig. 2). Over large parts of this area, the very resistant, quartz-cemented sandstones are exposed in large tilted rock faces that allow detailed observations from the sub-mm to km scale.

4. Data and methods

We measured and correlated eighteen detailed stratigraphic sections of 50 to 700 m length on the southern, overturned limb of the Saddleback Syncline along approx. 15 km strike length (Fig. 3). At several locations, we constructed facies maps. Approximately fifty slabbed and polished samples supplemented the field observations and were used for detailed observations, thin sectioning, and photography of microbial mat textures and morphologies. Paleocurrent data were mainly measured on planar and trough-cross stratified sandstones; data from clast imbrication and ripple crest orientation were used only in a few cases. All measurements were corrected for tectonic fold plunge and tilt of bedding using the structural parameters listed by Heubeck and Lowe (1994a). Rose diagrams were constructed using Stereonet 8.9.1 (Allmendinger et al., 2012). Grain size measurements of polished thin sections were performed by using the software ImageJ 1.49n. Relative coordinates, orientation, and the apparent long and short axis length of each resolvable grain were recorded for more than 3000 grains. Elemental mapping of polished rock chips was performed using a Horiba XGT-7000 X-ray fluorescence microanalyzer with a spatial resolution of 10 µm at Texas A&M University.

5. Stratigraphy and facies of the Saddleback Syncline

The investigated strata expose a variety of abundant and well-preserved sedimentary structures which allow interpretation of hydrodynamic processes and detailed reconstruction of paleoenvironments. They show only minor and localized brittle deformation and are crosscut by diabase dikes dated at ca. 2950 Ma (Klausen et al., 2010) and one prominent postdepositional strike-slip fault with an estimated offset of approx. 600 m (Fig. 3). Based on lithological composition, characteristic sedimentary structures and textures, internal and external geometries and vertical facies relationships, five major depositional facies can be distinguished (Fig. 3, Table 1). All following descriptions and interpretations refer to the Saddleback Syncline.

5.1. Facies 1

5.1.1. Description

The Moodies basal conglomerate (MdB) overlies felsic volcanic and volcaniclastic rocks of the Schoongezicht Formation of the Fig Tree Group with gradational contact and thins to the southwest (Heubeck and Lowe, 1994a). It is a polymict, clast-supported, pebble-and-cobble conglomerate, commonly interbedded with lenses of sand-matrix-supported conglomerate and gravelly sandstone, which increase toward the top of this unit (Heubeck and Lowe, 1994b; Fig. 4A). Dominant sedimentary structures include clast imbrication and horizontal stratification.

5.1.2. Interpretation

The low compositional and textural maturity of this conglomerate and its rapid lateral changes in composition and thickness point to a proximal origin and indicate deposition in a braided fluvial to alluvial environment (Eriksson, 1978, 1980; Heubeck and Lowe, 1994a).

5.2. Facies 2

5.2.1. Description

Medium-bedded, poorly sorted, medium-to coarse-grained sandstones are confined to the lower part of the studied succession. Low-angle planar and trough cross bedding in which foresets reach up to 0.3 m in preserved height is abundant. Sandstones are commonly pebbly or cobbly. Wedge-shaped conglomerates (single-clast to < 0.6 m thick), predominantly composed of black or black-and-white-layered chert, but felsic porphyry clasts, altered ultramafic volcanic rock and BIF also occur (Fig. 4B). These units can be followed laterally for up to 150 m. Clast diameter ranges between 0.5 and 16.5 cm with a mean value of 6 cm (n=148). The conglomeratic sandstones are locally associated with desiccation cracks on thin, discontinuous mudstone partings (Fig. 7A). Minor erosional channels up to 50 cm wide and up to 20 cm deep are filled by basal pebble lags overlain by trough-cross-bedded sandstone (Fig. 4C). Paleocurrent measurements yield mainly directions oriented towards the NE or SW (Fig. 3).

5.2.2. Interpretation

Low-angle cross-stratification in sandstone and lenticular conglomerates suggest dominant upper flow-regime conditions under high shear stress and high to medium current velocities. Rare desiccation cracks indicate ponding of shallow bodies of standing water and subaerial

exposure. Altogether, these are common features on unvegetated coastal floodplains (Long, 2004; Heubeck, 2009; Fralick and Zaniewski, 2012). This facies is overlain and interfingers towards the northeast with intertidal deposits (Fig. 3).

5.3. Facies 3

5.3.1. Description

Thin-bedded, poorly sorted, medium- to coarse-grained sandstone occurs widely in the upper part of the studied strata. These are commonly subhorizontally laminated, weather recessively and occasionally show a fenestral fabric (Fig. 4D). This fabric is characterized by isolated, empty or chert-filled cavities, usually 1 - 20 mm across, which are commonly elongated parallel to bedding. Desiccation cracks on thin discontinuous mudstone partings, filled with coarse-grained sandstone, are also common (Fig. 4E).

5.3.2. Interpretation

Abundant desiccation cracks indicate that these strata were deposited in shallow to very shallow water in a low-energetic environment with occasional subaerial exposure. This may have occurred in an upper intertidal to supratidal setting which was periodically inundated (Terwindt, 1988). Fenestral fabrics commonly form in these environments e.g. due to entrapment of gas in the sediment, produced by the decay of buried organic matter (Gerdes, 2007, see section 6.4)

5.4. Facies 4

5.4.1. Description

Sandstones of this facies are moderately to poorly sorted, medium-to coarse-grained, rarely interbedded with pebble stringers and single pebbles, and commonly form sigmoidal foreset bundles (Fig. 4F) and sinuous-crested ripples. Small erosive channels of 10 - 20 cm in width and a few cm in depth, reactivation surfaces and herringbone cross stratification are also common (Fig. 4G). Individual foresets may be mud-draped and reach a maximum height of 0.5 m (Fig. 4H). Desiccation cracks are less abundant. The foresets show consistent bidirectional paleocurrent directions towards the NE and SW (Fig. 3).

5.4.2. Interpretation

Reversing currents, sigmoidal-shaped foresets, highly varying flow velocities at shallow water depths and channelization are indicative of intertidal settings (Alam et al., 1985; Kreisa and Moila, 1986; Terwindt, 1988; Eriksson and Simpson, 2004). Mud drapes, formed due to slack-water deposition during current reversals, also are good indicators for tidally-influenced environments (Eriksson et al., 2006; Nichols, 2009).

5.5. Subtidal facies

5.5.1. Description

The deposits of this facies are represented widely by resistantly weathering, thick-bedded, moderately to well sorted, medium-grained sandstones. The top of this facies was selected as the datum for correlation of the measured stratigraphic sections because the contact is readily recognizable in the field and has excellent lateral continuity (Fig. 3). Large-scale, low-angle planar foresets up to 4 m in preserved thickness (Fig. 5A) are characteristic; trough

cross bedding (0.2 - 0.4 m) is less common. Paleocurrent directions indicate an unidirectional flow to the NE and were reconstructed based on the orientation of foresets and straight-crested symmetrical- to asymmetrical ripples (Figs. 3 and 5B and C). Steep-sided symmetrical depressions, approximately 4 cm deep and 10 cm wide, are rare (Fig. 5D).

5.5.2. Interpretation

The large-scale foresets represent remnants of unidirectionally-migrating dunes forming sand ridges in the subtidal shoreface zone (Desjardins et al., 2012; Nichols, 2009). Such large, elongated sand bodies are usually oriented obliquely to the coastline and often generated near shorelines that experience strong tidal currents and storms (Stubblefield et al., 1984). Small and steep erosional depressions are tentatively interpreted as gutter casts, which form in shallow-marine environments due to unidirectional current flow, often triggered by storms, or by the passing of a tidal bore (Allen, 1984; Myrow, 1992; Johnson and Baldwin, 1996; Archer, 2013). Although the size and uniformity of the foresets could also be expected from an aeolian dune setting, the absence of diagnostic aeolian features such as inversely graded foresets, pin stripe lamination, low-angle truncation surfaces, interdune deposits or desiccation cracks make this interpretation unlikely (Fryberger and Schenk, 1988; Eriksson and Simpson, 1998; Simpson et al., 2012).

6. Identification and classification of microbial mats

The biomass of microbial mats is inevitably subject to degradation upon burial. If the decomposition of the organic matter remains incomplete, carbonaceous material (kerogen) will remain and delineate the former location of the mat as a lamina. However, commonly,

no organic material is preserved. In such cases, the former presence of a microbial mat can only be inferred indirectly through physical or chemical properties of the sediment, e.g., indications of resistance to erosion, cohesiveness, modified permeability and mat-related mineralization (Schieber, 1999, 2004; Schieber et al., 2007; Gerdes et al., 2000; Noffke et al., 2001; Noffke, 2010). The resulting tell-tale sedimentary features, such as a lamina-specific sorting, shrinkage cracks, microbial sand chips or gas domes, are commonly referred to as microbially-induced sedimentary structures (MISS; Noffke et al., 2001a; Gingras, 2002) or mat-related structures (MRS; Schieber et al., 2007; Eriksson et al., 2010). In the Moodies Group, microbial lamination occurs as black, dark green weathering, erosion-resistant, densely spaced, subparallel crinkly laminae. They show, as detailed below, specific surface textures and mat morphotypes, evidence of enhanced cohesiveness, and various features indicative of mat destruction, decay and mineralization. The two stratigraphically lowest occurrences of microbial mats occur ~350 m and ~190 m, respectively, above the top of the basal conglomerate in the southwestern and northeastern part of the Saddleback Syncline (Fig. 3). The overlying sedimentary succession, ~1000 m thick, contains rare to abundant, macroscopically visible microbial mats. The best exposed and laterally most continuous outcrops are found in the upper 700 m of this succession (Figs. 2 and 3). Two additional units with widespread, well-developed microbial mats occur in the stratigraphically higher units MdCh of Lowe et al. (2012) and at the base of unit MdQ2 of Anhaeusser (1976) in the upper part of the Moodies Group in the Saddleback Syncline (Fig. 2). In the following, we will limit our description to the main occurrences of microbial mats showing the most continuous lateral exposure. These largely coincide with the informal lithostratigraphic unit MdQ1 of Anhaeusser (1976).

6.1. Kerogenous laminae

6.1.1 Description

Black to dark green, 0.5 to 1 mm thick, wavy-crinkly laminations are spaced vertically several millimeters to centimeters apart, separating individual sandstone sets (Fig. 6A). The green weathering color of the kerogenous laminae is due to minor admixtures of fine-grained chlorite which forms, along with carbonate and quartz, the most abundant minerals in the thick siltstones of the Moodies Group (Fig. 2). The seemingly homogenous appearance of the laminae can be resolved at microscopic scale into individual, interweaving strands of black carbonaceous matter (Figs. 6B and C). Where not modified by subsequent early postdepositional processes, the laminae coat sandy and gravelly sedimentary structures including horizontal lamination, individual foresets, sand ripple packages and individual conglomerate clasts (Figs. 6A and 7A). Laminations are occasionally cracked and their margins bent upward. They are laterally continuous at outcrop-scale and consistently interbedded with fine- to coarse-grained, occasionally gravelly sandstones, rarely also with conglomerate stringers. Granulometric analysis demonstrates that detrital sand particles are typically fine- to medium-grained below a lamina, fine-grained within it, and medium- to coarse-grained above (Figs. 6B and C and Supplementary Fig. 1). Particle long-axes within the laminations are usually oriented paralell to bedding, whereas grains below and above the lamination are dominantly randomly oriented. Fine-grained heavy minerals, such as zircon and rutile or anatase are commonly enriched within the lamina (Fig. 6D). Notable is the near-complete absence of shale.

6.1.2. Interpretation

The morphological similarity of the wavy-crinkly laminae to modern and other fossil microbial mat laminae, their facies setting and the reported negative $\delta^{13}C$ isotope ratios of -20.1 ‰ to -22.5 ‰ PDB (Noffke et al., 2006) obtained from these kerogenous laminations are indicative of, and consistent with, a biogenic origin (Schidlowski, 2001). Negative $\delta^{13}C$ values can also be produced by abiotic processes, e.g., through Fischer-Tropsch-type reactions in hydrothermal environments or during the decomposition of siderite under metamorphic conditions (McCollom and Seewald, 2006, and references therein). However, the study area lacks any evidence for hydrothermal activity such as chert veining. The difference in grain size above and below the microbial lamina indicate changes in current velocity which may correspond to periods of enhanced mat growth during phases of reduced water flow velocity and clastic deposition (Noffke et al., 1997; Noffke, 2010). For the grain size distributions determined in thin section, the minimum flow velocities are approximately 0.08 m/s before, 0.06 m/s during, and 0.09 m/s after mat growth (calculated after Williams et al., 2013; Table S1 and S2, Supplementary Fig. 1). Observations of modern mat growth suggest that the development of thick mats is usually preceded by the establishment of biofilms during times of low hydrodynamic energy (Krumbein et al., 1994; Noffke et al., 1997). However, it is conceivable that a permanent sediment bypass was occuring during mat growth and only fine-sized particles and heavy mineral grains were trapped within the mat fabric. In contrast, the coarser-grained and poorly sorted sand layers immediately overlying the mats likely reflect depositional events in which current velocities were sufficiently high to transport them but not high enough to erode the mats. During subsequent periods of relative quiescence, the deposited sand was recolonized by microbes which either originated from the water column or migrated upwards from the buried mat

over a distance of millimeters to few centimeters (Noffke, 2010). Most laminae represent the rare case of *in situ* preserved microbial mats which were partly degraded, dehydrated and early cemented, but being only minimally compacted. The accumulation of detrital heavy minerals within the mat fabric, caused by microbial baffling and trapping, is common in epibenthic microbial mats (Gerdes et al., 2000). Consequently, heavy mineral laminations can be indicative of ancient mats and thus could serve as biosignatures where no organic matter has been preserved (Noffke, 2010).

6.2. Mat morphotypes and their relationship to siliciclastic facies

6.2.1 Description

Environmental parameters inferred from physical sedimentary structures (Table 1) constrain the habitat and biological affinity of the microbial community. Based on our field observations, microbial mats can be assigned to three different paleoenvironments, each associated with a specific mat morphotype:

(1) Planar microbial mats, without any significant morphological relief, are typical of the coastal floodplain zone (section 5.2; Fig. 7A). Vertically-oriented growth structures (e.g., microbial domes) are absent. However, laminae occasionally onlap, drape and overgrow thin pebble and cobble conglomerate beds and may occur a few millimeters above and below thin, desiccation-cracked bedding planes (Fig. 7A).

(2) Wavy-crinkly microbial mats, which are commonly associated with bedding-plane-parallel chert layers, dominate the intertidal zone (section 5.4; Fig. 7B). These layers widely contain remnants of carbonate minerals (see description below in section 6.2.5). Microbial laminae

coat sand ripples and cross-laminations and occasionally form small, isolated microbial domes showing increased lamina density. These preferentially develop on minor topographic highs (Fig. 8A). Small channels filled by coarse-grained sandstone fill the relief defined by microbial domes (Heubeck, 2009).

(3) Tufted microbial mats are exclusively present in strata that are inferred to represent upper inter- to supratidal facies (section 5.3; Fig. 7C). The tufts are typically 0.3 - 1 cm in height but can attain up to 2 cm where they are vertically stacked in cones (Fig. 7C). Tufts are spaced several centimeters apart and are laterally supported by draping laminae (Figs. 8B and D). Tufts are sub-circular in horizontal section (Fig. 8E) and internally filled with fine-grained sediment. Some, however, are filled by nodular microcrystalline quartz (Figs. 8B and F and 9A). The density of the kerogenous lamina seemingly increases within the silicified tuft (Figs. 8D and F).

6.2.2. Interpretation

The growth of these three distinct mat morphotypes presumably represents a morphological response of mat-building microbial communities to changing physicochemical conditions (Gerdes et al., 1993, 2000; Battin et al., 2003; Eriksson et al., 2010). The tufted mats, in particular, resemble closely modern tufted microbial mats from Bahar Alouane (Tunisia) that are dominantly built by filamentous cyanobacteria that intertwine and form durable networks of reticulate ridges on the sediment surface (Fig. 8C, see discussion below in section 7.4). The nodular chert in the interior of some tufts most likely represent the fill of former gas bubbles that were trapped within the mat fabric, which is well-known from

modern cyanobacterial mats that produce oxygen-rich bubbles with strikingly similar morphologies (Figs. 8F and 9A and B; Bosak et al., 2010). Microbial tufts and domes in the studied Moodies strata occur confined to the tidally-influenced facies and exhibit almost vertical structures, well above the critical angle of repose for sand grains. These delicate vertical structures appear to have been solely formed and structurally supported by biomass but probably would not have been preserved without early silicification.

6.3. Mat destruction and cohesiveness

6.3.1. Description

Microbial mat-covered sediment surfaces in the upper inter- to supratidal facies occasionally show polygonal or incomplete networks of cracks with slightly upward-curved margins and sand-filled openings which can be traced over several cm length (Fig. 10A). These cracks are commonly associated with, but distinct from, more prominent desiccation-cracked mudstone layers (compare Figs. 6A and 10B). Occasionally, eroded fragments of mat-bound sediment are incorporated in the shallow and wide channels between cross-bedded sandstones as 1 - 5 mm-thick, ~2 - 9-cm-long, ridged and slightly curved clasts (Figs. 10C, D and E), forming microbial-sand-chip conglomerates (Pflüger and Gresse, 1996; Eriksson et al., 2007).

6.3.2. Interpretation

Periods of persistent subaerial exposure dehydrate mats, leading to their shrinkage and cracking. The resulting microbial mat chips easily peel off the sandy substrate, are transported by wind or reworked by flowing water and redeposited during flood events (Noffke, 1999; Schieber, 2004; Bouougri and Porada, 2012). Curved and upturned ends of

some chips indicate a moderate elasticity while desiccating; however, roll-up structures noted by Noffke et al. (2006) have not been observed. Apparently, the mat chips had a high rigidity even under turbulent flow. These observations indicate a tough, perhaps leather- or rubber-like consistency, possibly enhanced by early silicification (Schieber, 2004; Tice et al., 2011).

6.4. Mat decay

6.4.1. Description

In some sandstone beds, microbial mats are disrupted and bent upwards along subvertical linear structures that trend perpendicular to bedding and reach dm to m in height (Fig. 11A). These structures occur throughout the studied succession are laterally unevenly spaced, but are restricted to microbial mat-bearing sandstones (Fig. 3). They are particularly common in a ~50-m-thick, densely microbial-mat-laminated section in the upper parts of the MdQ1 unit which can be traced for >7 km in strike length in strata interpreted as upper inter- to supratidal facies (Fig. 3). In this section, the vertical linear structures occur in medium-to coarse-grained, thin-bedded sandstone. The central area of the subvertical channels shows thread-like, disrupted dark, carbonaceous material and occasionally nodular chert (Fig. 11A and Supplementary Fig. 2). Where the linear structures intersect bedding planes, they form a pattern of polygonal cracks of 1 - 5 cm width and several dm length, bordered by two parallel running ridges (Fig. 11B). The mean vertical extent of 62 surveyed structures in the upper inter- to supratidal facies of the study area is 2.1 m, the maximum height is 6.1 m. The structures are less common in the coastal floodplain and intertidal facies and also smaller. There they reach mean heights of only 0.2 and 0.4 m, respectively (Table 1). Subcircular, ~1 -

2 cm-high and ~2 - 8 cm-wide mounds with a prominent central depression locally appear on microbial-mat-covered bedding planes in sandstones with common fenestral fabric, assigned to the supratidal facies (Fig. 11C).

6.4.2. Interpretation

The vertical linear structures bordered by upward-curved mats are best explained as gas- or fluid-escape structures formed in mat-bound sediment in a postdepositional, but early diagenetic stage, indicated by the plastic behavior of the unconsolidated sediment and by the absence of mud (Lowe, 1975; Eriksson, 1979; Heubeck, 2009). Experimental studies of Frey et al. (2009) define a key morphological difference between gas- and water-escape structures: laminations warp downward when deformed by water fluidization but upward when disturbed by gas fluidization as is the case in the examples studied here. The circular mounds with the central depression likely represent smaller, ruptured gas domes and should not be confused with sand volcanoes which are the result of purely physical processes, occuring e.g. during the rising flood in supratidal settings (Dornbos et al., 2007; Taj et al., 2014). Surface sealing by mats which hinder the escape of biogenic gas that either developed from buried organic matter, or was related to metabolic effects of live microbial mats, can trigger the formation of fenestral fabric, gas domes and escape structures (Gerdes et al., 1993, 2000; Gerdes, 2007; Noffke et al., 2001b; Bose and Chafetz, 2009). However, fluid escape due to the dewatering of compacting mats and sediment cannot be ruled out. The cracks observed on mat-covered bedding planes may form part of larger polygonal crack networks in brittle, superficially cemented sediment through which gas or water escaped. Similar polygonal crack patterns are common in modern uper inter- to supratidal mats (Noffke et al., 2001a; Gerdes, 2007; Noffke, 2010; Bouougri and Porada, 2007; Bose and Chafetz, 2009).

6.5. Mat-associated mineralization

6.5.1. Description

Microbial mats in the intertidal zone are widely underlain by bedding-plane-parallel chert layers that are a few mm thick, up to 80 cm long and gradually thin laterally (Figs. 7B and 12A and B). In cross- section, these layers show gently undulating upper contacts whereas the contact with the underlying sediment is commonly more irregular (Fig. 7B). The chert layers are never eroded nor erosive and contain remnants of carbonate minerals. In places, ferroan dolomite makes up more than half of the layers (Figs. 12A and B). It clearly displays corroded and undulatory grain boundaries, and truncated dolomite twin lamellae, as well as abundant nucleation centers of chert (Fig. 12C). Gamper et al. (2012) also described undulating wisps of kerogenous laminations within the chert layers.

6.5.2. Interpretation

The occurrence of chert layers a few mm underneath the microbial mats indicates that their formation may be related. Because chert layers are never eroded nor reworked, they likely formed post-depositionally in the shallow subsurface. Hence, the previous interpretation, namely, that these chert layers formed at the sediment-water or sediment-atmosphere interface and may represent very-early-mineralized, patchy microbial mats (suggested by Heubeck, 2009, and by Gamper et al., 2012) now appears less likely. The apparent replacement of carbonate by chert rather suggests that primary carbonates had precipitated

in synsedimentary cavities that developed beneath the microbial mats and were dissolved when pore waters became acidic, which promoted the precipitation of silica. Both processes would also explain the excellent preservation of the delicate microbial tufts. Carbonate precipitation is common in modern photosynthetic mats and is frequently interpreted to be induced through metabolic activity and/or templating of nucleation (Burne and Moore, 1987; Reid et al., 2000; Dupraz et al., 2009; Decho, 2010).

7. Discussion

7.1. Facies

Paleoenvironmental reconstructions and facies analysis of Archean depositional systems are often hampered by poor preservation, diagenetic, and metamorphic overprint or post-depositional tectonics (Eriksson et al., 1998; Altermann and Corcoran, 2002; Donaldson et al., 2004; Embry et al., 2004; Van Kranendonk et al., 2007; Wacey, 2009).

In the Saddleback Syncline of the central BGB, however, the outstanding exposure, abundant well-preserved sedimentary structures, high temporal resolution, excellent lateral continuity and only minor metamorphic and tectonic overprint provide a reliable basis for paleoenvironmental reconstructions of Moodies strata, which record the transition from alluvial-braided fluvial to a peritidal shoreline setting, followed by subtidal, then upper inter- to supratidal depositional environments. Two vertical facies trends can be noted in this succession: a deepening- and fining-upward trend from alluvial to subtidal facies, followed by an aggradational, largely shallow-marine upper inter- to supratidal facies. Correlation of measured sections indicates only minor lateral facies changes in the plane of exposure;

rather, the overall horizontal superposition of strata reflects an overall aggradational stacking pattern in which subsidence and sediment supply were well balanced.

The most prominent change along strike is a decrease in the number and thickness of thin conglomeratic stringers towards the NE, concomitant with an increase in the thickness of the subtidal facies. This may indicate a southwestern provenance of these sediments. Measured paleocurrents are mostly oriented towards the NE and SW in tidally-influenced strata, and towards the NE and E in the subtidal facies (Fig. 3). The predominant transport direction of the investigated sandstone succession in the lower half of the Saddleback Syncline is directed towards the NE (Fig. 3). These observations disagree with previous paleoflow reconstructions of Heubeck and Lowe (1994a, 1999), which had indicated an overall SW-oriented transport direction in the Saddleback Syncline.

A possible explanation for the observed lack of significant lateral facies changes is that the subvertical dip allows easy recognition of foresets indicating sediment transport subparallel to depositional strike but makes it difficult to recognize across-strike transport facies change. The apparent low variability in facies changes also indicates that the sedimentary basin(s) of early Moodies time and north of the Inyoka Fault, was (or were) only poorly confined by the present tectonic boundaries; they presumably extended well beyond the present-day boundaries of the BGB (Heubeck and Lowe, 1999). A generalization of the observation would suggest that Archean continents and their shelves may have been covered for several tens of kilometers by extensive coastal zones due to an overall low topographic gradient, combined with low continental freeboard (Eriksson, 1999; Eriksson et al., 2004). Consequently, substantial lateral facies changes in the terrestrial, coastal, and nearshore zones could only be observed at a large scale.

7.2. Biogenicity

Decades of research and the development of sophisticated techniques have led to the establishment of a number of solid criteria for assessing the biogenicity and syngenicity of purported evidence of life (Schopf, 1993, 2004, 2006; Brasier et al., 2002, 2006; Schopf and Kudryavtsev, 2005, 2009; Wacey, 2009; Wacey et al., 2010, 2012, 2014). Below, we will follow mainly those laid down by Schopf (2004) and Brasier et al. (2006). Geological context, age, facies, and provenance of the microbial mat-bearing sandstones of the Moodies Group are reasonably well constrained (Heubeck and Lowe, 1994a; Heubeck, 2009; Heubeck et al., 2013). The observations described above document a close interaction between the kerogenous laminae and associated small- and medium-scale sedimentary structures in Moodies sandstones, reflecting also facies changes. The syndepositional origin of the laminae is unquestionable (Schieber, 2004). At outcrop scale, changes in dominant mat morphotype correlate well with changes in clastic facies, which suggests an adaptation of the microbial mats to the environment and therefore serve as a biogenicity indicator (Allwood et al., 2006; Brasier et al., 2006). At microscale, negative $\delta^{13}C$ values of the kerogen and associated filamentous microstructures are indicative of a microbial origin (Noffke et al., 2006; Gamper et al., 2012; Homann et al., 2013). Consequently, the laminae do not represent abiogenic deposits of organic matter on the sedimentary surface, e.g., by fall-out deposits from atmospheric haze or marine colloids that were subsequently concentrated and deformed during early diagenesis (Wells, 1998; Trainer et al., 2006). No known abiological process can explain the systematic variations and observed correlations between the kerogenous laminations and their surrounding siliciclastic substrate. Rather, the steepness of the near-vertical, up to 1 cm-high microbial tufts and the widespread occurrence of the kerogenous laminae is consistent with a primary, microbially-mediated,

erosion-resistant relief on the paleosurface, subsequently locally deformed by upward-migrating gases and/or fluids, or locally eroded and incorporated in mat-chip conglomerates.

7.3. Biostratigraphy and paleoecology

Biostratigraphy based on microbial-mat morphology, associated mat-related structures, and comparisons with modern analogs allows to spatially refine paleoenvironmental interpretations (Table 1; Banerjee et al., 2014; Sarkar and Banerjee, 2014). Similar approaches have been conducted on the basis of morphological differences of stromatolites, providing a more precise interpretation of their paleoenvironmental context (Schopf, 1977; Bertrand-Sarfati and Walter, 1981; Allwood et al., 2006; Grey et al., 2011; Jahnert and Collins, 2012, 2013). Morphological relief does not necessarly correlate with an increased bioproductivity, however, it can be assumed that it indicates an increased biomass accumulation. Large amount of biomass accumulation could either indicate high bioproductivity or low biomass degradation.

Microbial mats of the Moodies Group are morphologically most prominent and show the highest topographic relief in the *upper inter- to supratidal facies*, suggesting optimal growth conditions and bioproductivity there. Tufted microbial mats are widespread in this facies and occur in association with gas domes, giant gas- or fluid-escape structures, and shrinkage cracks. In contrast, tufts, gas domes, and shrinkage cracks are mostly absent in the adjacent *intertidal facies*, which are dominated by wavy-crinkly mat morphologies and relatively small microbial domes. Their wavy morphology could have been enhanced by a preexisting topography such as, e.g., ripples and forests. A subsequent and repeated mat overgrowth of topographic highs could have caused the development of microbial domes that might

represent initial growth stages of tufts. Mats in this facies are typically associated with abundant mat chips and chert layers while gas-/or fluid-escape structures are distinctly subordinate. In the *coastal floodplain facies* only a small variety of mat-related structures has been observed. Mats typically display a planar and generally less complex morphology which is likely a morphological adaptation to high hydrodynamic shear stress. We have not identified microbial mats or mat-related structures either in the *braided fluvial to alluvial facies* or *subtidal facies* of the Moodies Group, which might be either due to reduced preservation potential and poorer development there or due to the primary absence of microbial mats.

A similar distribution pattern of mat-related structures and mat morphotypes, especially tufted mats, have been reported from other siliciclastic strata of Precambrian age (Banerjee et al., 2014) as well as from modern environments (Gerdes et al., 2000; Cuadrado et al., 2011; Bose and Chafetz, 2009; Sarkar and Banerjee, 2014). Mat morphotypes described above likely represent an active adaptation by the microbial community to environmental factors such as sedimentation rate, hydrodynamic regime, and the availability of nutrients and light (e.g., Gerdes et al., 2000). It is important to note that these adaptations are not found at point sources such as hydrothermal vents but occur regionally and developed exclusively in the shallow- and very shallow-water photic zone of the Moodies Group under conditions of moderate to high water agitation. This not only indicates that this environment represented an ecological optimum for the growth and preservation of the mats but also strongly suggests that these communities were phototrophic and able to sustain the presumably high UV radiation (Phoenix et al., 2001). The reported $\delta^{13}C$ values of -20.1 ‰ to -22.5 ‰ (Noffke et al., 2006) are in the range of cyanobacteria, however, similar values can also be produced by anoxygenic phototrophs or methanogens (Schidlowski,

2001; Schopf, 2011). A methanotrophic-bacteria-dominated community is rather unlikely because their $\delta^{13}C$ values would be significantly more negative.

7.4. Tufted microbial mats

Tufted mats of the inferred upper inter- to supratidal zone in the Moodies Group are strikingly similar to modern tufted mats, which are predominantly built by filamentous cyanobacteria and described, e.g., from Bahar Alouane, Tunisia (Fig. 8C; Gerdes et al. 2000, Gerdes, 2007), Shark Bay, Australia (Jahnert and Collins, 2013), Texas Gulf Coast, USA (Bose and Chafetz, 2009), and the Red Sea of Saudi Arabia (Taj et al., 2014). Polygonal patterns of reticulate ridges with tufts at ridge junctions are a well known surface texture in modern (e.g., Gerdes, 2007; Shepard and Sumner, 2010) and some Archean tufted mats (Beukes, 1987; Sumner, 1997; Flannery and Walter, 2011). Due to the steep dip throughout the study area, only a limited amount of bedding planes are exposed. However, tufts in cross-section view can be seen to be laterally connected by draping lamina which either represent ridges or a transect through a continuous mat cover (Fig. 8B and D).

The process of tuft formation in modern settings is not entirely understood. It is thought to require gliding motility and tangling behavior of the mat-building filaments. Tufts and cones have been interpreted to indicate microbial phototatic behavior but this process remains debated (Castenholz, 1968, 1967; Walter et al., 1976; Shepard and Sumner, 2010; Bosak et al., 2012; Sim et al., 2012; Reyes et al., 2013). Morphogenetic mechanisms such as photo- and chemotaxis, competition for space, potentially mediated by quorum sensing may also be involved (Petroff et al., 2010; Decho, 2010). Tuft formation may be a communal microbial strategy to penetrate the laminar boundary layer in the flowing medium above the substrate,

gaining access to the overlying, more nutrient-laden turbulent layer (Tice et al., 2011). To date, the oldest fossil tufted microbial mats are reported from the 2.7 Ga Tumbiana Fm., Australia (Flannery et al., 2011). The putative micro-tufted structures described by Noffke et al. (2013) from the 3.48 Ga Dresser Fm., Australia, reach only 25 - 50 µm in height (Fig. 6 of Noffke et al., 2013), are thus at another scale of observation and therefore, in our opinion, not comparable with the macroscopic, 0.3-to-1 cm-high microbial tufts (Fig. 8) preserved in Moodies sandstones. Hence, the Moodies Group contains the oldest known convincing macro-tufted microbial mats in the geological record.

High resistance and adaptability to environmental stresses, high productivity, and the ability to form and sustain complex vertical structures only supported by biomass is an almost unique trait of cyanobacteria (Lyons and Kolter, 2015). Phylogenetic analysis suggest that the ancestor to most extant cyanobacteria evolved between 2.4 - 3.1 Ga or even earlier (Schirrmeister et al., 2013). Bosak et al. (2009) linked the formation of oxygen-rich bubbles in modern cyanobacterial cones with fossil gas bubbles present in the central zone of 2.7 Ga conical stromatolites and concluded that fossil gas bubbles may be used as an indicator for oxygenic photosynthesis. Moreover, experiments with laboratory-grown cyanobacterial mats propose that tufted structures can serve as morphological indicator of oxygenated Archean environments (Sim et al., 2012). Therefore, in the absence of preserved biomarkers in the Moodies Group the morphological attributes of the microbial mats may be the principal clue to constrain the microbial metabolism(s). If cyanobacteria were indeed the only microorganisms with the ability to form macroscopic tufts, their first appearance in the geological record would set a minimum age for the origin of cyanobacteria. This reasoning has been previously made by Flannery et al. (2011) and would now place their origin to at least 700 Ma prior to the GOE.

7.5. Regional and stratigraphic distribution

Fossilized microbial mats appear to be absent in shallow-water paleoenvironments of other large Moodies synclines north of the Inyoka Fault, such as the Eureka Syncline, the Moodies Hills Block, and the Stolzburg Syncline, even though we conducted careful dedicated searches in stratigraphically equivalent units there; microbial mats have been found only in the Saddleback and Dycedale Synclines and possibly thin and poorly developed ones in the Stolzburg Syncline. Microbial mats have not been documented from the quartzose sandstones of the Moodies Group south of the Inyoka Fault. This apparent absence is puzzling because the abundant sedimentary structures and common sandy, silty, and gravelly lithologies in the stratigraphically equivalent units in these tectonic regions strongly suggest equivalent facies, ranging between braided-stream and prodelta. The absence of microbial mats may be explained by either one or a combination of two hypotheses: (1) Mats did not form elsewhere because environmental conditions there were subtly different and growth conditions unfavorable to allow macroscopic accumulation; (2) microbial mats were not preserved elsewhere because only the Moodies strata in the central Saddleback Syncline in the interior of the BGB experienced the proper combination of very early silicification, low tectonic strain and low hydrothermal overprint, thus preserving the organic matter.

8. Conclusions

Microbial mats of the 3.22 Ga Moodies Group, exposed on the overturned limb of the Saddleback Syncline, represent one of Earth's oldest, macroscopically visible, large-scale and mappable Archean ecosystem. The fossil mats are preserved as kerogenous laminations and are particularly unique due to their excellent preservation and large extent over approx. 15 km strike length in a stratigraphically coherent interval of roughly 1000 m thickness. Microbial mat biostratigraphy based on (1) mat morphology (planar, wavy, and tufted), (2) the association and distribution pattern of distinct microbial-mat-related structures, and (3) comparisons with modern analogs was applied for spatially refining the paleoenvironmental settings. In the coastal floodplain zone, mats are typically planar, whereas the association of more complex wavy-crinkly mat morphotypes, small microbial domes, and mat chips is characteristic for the intertidal zone. Tufted microbial mats are exclusively present in the upper inter- to supratidal zone and are commonly associated with shrinkage cracks, gas domes, and extensive gas- or fluid-escape structures. These three distinct mat morphotypes are interpreted to represent an adaptation of the phototrophic microbial communities to changing physiochemical conditions, furthermore, the tufted microbial mats were perhaps build by ancestral cyanobacteria. These microbial communities had optimum growth conditions in the photic zone under moderate water agitation and persisted within mechanically abrasive, high-energy shoreline environments.

Acknowledgements

Research was supported by DFG grant He2418/13-1. CH was partially supported by the EU COST Action "Life-ORIGINS" (TD1308). MH and CH thank Jonathan Engelhardt, Laura

Stutenbecker, Nadja Drabon, Sami Nabhan, Danielle Zentner and Lizzy Trower Stefurak for assistance in the field. The authors are grateful to Sappi Limited and their forestry managers for permission to access private forest roads. We thank Don Lowe, Gary Byerly, Martin Van Kranendonk, Kurt Konhauser, Bill Schopf, Jian Gong, David Flannery, and Tomaso Bontognali for constructive discussions and comments on various aspects of this work. The Nel family provided help and hospitality. Anna Giribaldi, FU Berlin, prepared thin sections; Tim Luber and Markus Gogouvitis are thanked for helping with sample preparation; Daniel Korb and Oliver Burkhardt assisted in the grain size analysis. Thoughtful and constructive reviews by Martin Van Kranendonk and an anonymous reviewer significantly improved the manuscript.

References

Alam, M.M., Crook, K.A.W., Taylor, G., 1985. Fluvial herring-bone cross-stratification in a modern tributary mouth bar, Coonamble, New South Wales, Australia. Sedimentology 32, 235–244. doi:10.1111/j.1365-3091.1985.tb00506.x

Allen, J.R.L., 1984. Sedimentary structures: their character and physical basis, in: Developments in Sedimentology 30. Elsevier, Amsterdam, p. 663.

Allmendinger, R.W., Cardozo, N.C., Fisher, D., 2012. Structural Geology Algorithms: Vectors & Tensors, Structural Geology Algorithms. Cambridge University Press, Cambridge.

Allwood, A.C., Walter, M.R., Kamber, B.S., Marshall, C.P., Burch, I.W., 2006. Stromatolite reef from the Early Archaean era of Australia. Nature 441, 714–8. doi:10.1038/nature04764

Altermann, W., Corcoran, P.L., 2002. Precambrian Sedimentary Environments: A modern approach to ancient depositional systems. Blackwell Science (Special publication number 33 of the International Association of Sedimentologists), Oxford.

Anbar, A.D., Duan, Y., Lyons, T.W., Arnold, G.L., Kendall, B., Creaser, R., Kaufman, A.J., Gordon, G.W., Scott, C., Garvin, J., Buick, R., 2007. A whiff of oxygen before the great oxidation event? Science 317, 1903–6. doi:10.1126/science.1140325

Anhaeusser, C.R., 1976. The geology of the Sheba Hills area of the Barberton Mountain Land, South Africa: with particular reference to the Eureka Syncline. Trans. Geol. Soc. S. Afr 79, 253–280.

Archer, A.W., 2013. World's highest tides: Hypertidal coastal systems in North America, South America and Europe. Sediment. Geol. 284-285, 1–25. doi:10.1016/j.sedgeo.2012.12.007

Banerjee, S., Sarkar, S., Eriksson, P.G., 2014. Palaeoenvironmental and biostratigraphic implications of microbial mat-related structures: Examples from the modern Gulf of Cambay and the Precambrian Vindhyan. J. Palaeogeogr. 3, 127–144. doi:10.3724/SP.J.1261.2014.00048

Battin, T.J., Kaplan, L.A., Newbold, J.D., Hansen, C.M.E., 2003. Contributions of microbial biofilms to ecosystem processes in stream mesocosms. Nature 439–442.

Bertrand-Sarfati, J., Walter, M.R., 1981. Stromatolite biostratigraphy. Precambrian Res. 15, 353–371.

Beukes, N.J., 1987. Facies relations, depositional environments and diagenesis in a major Early Proterozoic stromatolitic carbonate platform to basinal sequence, Campbellrand Supergroup, Transvaal Supergroup, Souhhern Africa. Sediment. Geol. 54, 1–46.

Bontognali, T.R.R., Fischer, W.W., Föllmi, K.B., 2013. Siliciclastic associated banded iron formation from the 3.2Ga Moodies Group, Barberton Greenstone Belt, South Africa. Precambrian Res. 226, 116–124. doi:10.1016/j.precamres.2012.12.003

Bosak, T., Bush, J.W.M., Flynn, M.R., Liang, B., Ono, S., Petroff, a. P., Sim, M.S., 2010. Formation and stability of oxygen-rich bubbles that shape photosynthetic mats. Geobiology 8, 45–55. doi:10.1111/j.1472-4669.2009.00227.x

Bosak, T., Liang, B., Sim, M.S., Petroff, A.P., 2009. Morphological record of oxygenic photosynthesis in conical stromatolites. Proc. Natl. Acad. Sci. U. S. A. 106, 10939–10943. doi:10.1073/pnas.0900885106

Bosak, T., Liang, B., Wu, T.-D., Templer, S.P., Evans, A., Vali, H., Guerquin-Kern, J.-L., Klepac-Ceraj, V., Sim, M.S., Mui, J., 2012. Cyanobacterial diversity and activity in modern conical microbialites. Geobiology 10, 384–401. doi:10.1111/j.1472-4669.2012.00334.x

Bose, S., Chafetz, H.S., 2009. Topographic control on distribution of modern microbially induced sedimentary structures (MISS): A case study from Texas coast. Sediment. Geol. 213, 136–149. doi:10.1016/j.sedgeo.2008.11.009

Bouougri, E., Porada, H., 2007. Complex structures associated with siliciclastic biolaminites, in: Schieber, J., Bose, P.K., Eriksson, P.., Banerjee, S., Sarkar, S., Altermann, W., Catuneanu, O. (Eds.), Atlas of Microbial Mat Features Preserved within the Siliciclastic Rock Record. Elsevier, Amsterdam, pp. 111–115.

Bouougri, E., Porada, H., 2012. Wind-induced mat deformation structures in recent tidal flats and sabkhas of SE-Tunisia and their significance for environmental interpretation of fossil structures. Sediment. Geol. 263-264, 56–66. doi:10.1016/j.sedgeo.2011.12.011

Brasier, M., Green, O.R., Jephcoat, A.P., Kleppe, A.K., Van Kranendonk, M., Lindsay, J.F., Steele, A., Grassineau, N.V., 2002. Questioning the evidence for Earth's oldest fossils. Nature 416, 76–81.

Brasier, M., McLoughlin, N., Green, O., Wacey, D., 2006. A fresh look at the fossil evidence for early Archaean cellular life. Philos. Trans. R. Soc. Lond. B. Biol. Sci. 361, 887–902. doi:10.1098/rstb.2006.1835

Buick, R., 2008. When did oxygenic photosynthesis evolve? Philos. Trans. R. Soc. Lond. B. Biol. Sci. 363, 2731–43. doi:10.1098/rstb.2008.0041

Burne, R.V.R. V, Moore, L.S.L.S., 1987. Microbialites : Organosedimentary Deposits of Benthic Microbial Communities. Palaios 2, 241–254.

Byerly, G.R., Lowe, D.R., Walsh, M.M., 1986. Stromatolites from the 3,300–3,500-Myr Swaziland Supergroup, Barberton Mountain Land, South Africa. Nature 319, 489–491.

Castenholz, R.W., 1967. Aggregation in a thermophilic Oscillatoria. Nature 215, 1285–1286.

Castenholz, R.W., 1968. The behavior of Oscillatoria terebriformis in hot springs. J. Phycol. 4, 132–139.

Condie, K.C., 1997. Plate Tectonics and Crustal Evolution, 4th ed. Butterworth-Heinemann, Oxford.

Crowe, S.A., Døssing, L.N., Beukes, N.J., Bau, M., Kruger, S.J., Frei, R., Canfield, D.E., 2013. Atmospheric oxygenation three billion years ago. Nature 501, 535–8. doi:10.1038/nature12426

Cuadrado, D.G., Carmona, N.B., Bournod, C., 2011. Biostabilization of sediments by microbial mats in a temperate siliciclastic tidal flat, Bahia Blanca estuary (Argentina). Sediment. Geol. 237, 95–101. doi:10.1016/j.sedgeo.2011.02.008

De Ronde, C.E.J., De Wit, M.J., 1994. Tectonic history of the Barberton Greenstone Belt, South Africa: 490 million years of Archaean evolution. Tectonics 983–1005.

De Ronde, C.E.J., Hall, C.M., York, D., Spooner, E.T.C., 1991. Laser step-heating 40Ar/39Ar age spectra from Early Archean (~3.5 Ga) Barberton greenstone belt sediments: A technique for detecting cryptic tectono-thermal events. Geochim. Cosmochim. Acta 55, 1933–1951.

De Ronde, C.E.J., Kamo, S.L., 2000. An Archaean arc-arc collisional event: A short-lived (ca 3 Myr) episode, Weltevreden area, Barberton greenstone belt, South Africa. J. African Earth Sci. 30, 219–248. doi:10.1016/S0899-5362(00)00017-8

De Wit, M.J., Furnes, H., Robins, B., 2011. Geology and tectonostratigraphy of the Onverwacht Suite, Barberton greenstone belt, South Africa. Precambrian Res. 186, 1–27.

Decho, A.W., 2010. Overview of biopolymer-induced mineralization: What goes on in biofilms? Ecol. Eng. 36, 137–144. doi:10.1016/j.ecoleng.2009.01.003

Desjardins, P.R., Buatois, L.A., Ma, M.G., 2012. Tidal Flats and Subtidal Sand Bodies, in: Knaust D., Bromley R. (Eds.), Trace Fossils as Indicators of Sedimentary Environments. Elsevier, pp. 529–561.

Donaldson, J.A., Aspler, L.B., Chiarenzelli, J.R., 2004. Sedimentary Structures: An essential key for interpreting the Precambrian rock record, in: Eriksson, P.G., Altermann, W., Nelson, D.R., Mueller, W.U., Catuneanu, O. (Eds.), The Precambrian Earth: Tempos and Events. Elsevier (Developments in Precambrian Geology), Amsterdam, pp. 602–612.

Dornbos, S.Q., Noffke, N., Hagadorn, J.W., 2007. Mat-decay features, in: Schieber, J., Bose, P.K., Eriksson, P.., Banerjee, S., Sarkar, S., Altermann, W., Catuneanu, O. (Eds.), Atlas of Microbial Mats Features …. Elsevier, Amsterdam, pp. 106–110.

Dupraz, C., Reid, R.P., Braissant, O., Decho, A.W., Norman, R.S., Visscher, P.T., 2009. Processes of carbonate precipitation in modern microbial mats. Earth-Science Rev. 96, 141–162. doi:10.1016/j.earscirev.2008.10.005

Embry, A.F., Catuneanu, O., Eriksson, P.G., 2004. Sequence stratigraphy and the Precambrian, in: Eriksson, P.G., Altermann, W., Nelson, D.R., Mueller, W.U., Catuneanu, O. (Eds.), The Precambrian Earth: Tempos and Events. Elsevier (Developments in Precambrian Geology), Amsterdam, pp. 681–684.

Eriksson, K.A., 1977. Tidal deposits from the Archaean Moodies Group, Barberton Mountain Land, South Africa. Sediment. Geol. 18, 257–281.

Eriksson, K.A., 1978. Alluvial and destructive beach facies from the Archaean Moodies Group, Barberton Mountain Land, South Africa and Swaziland, in: Miall, A.D. (Ed.), Fluvial Sedimentology. Can. Soc. Petrol. Geol., Mem. 5, pp. 287–311.

Eriksson, K.A., 1979. Marginal marine depositional processes from the Archaean Moodies Group, Barberton Mountain Land; South Africa: Evidence and significance. Precambrian Res. 8, 153–182.

Eriksson, K.A., 1980. Transitional sedimentation styles in the Fig Tree and Moodies Group, Barberton Mountain Land, South Africa: evidence favouring an Atlantic or Japan sea-type Archaean continental margin. Precambrian Res. 12, 141–160.

Eriksson, K.A., Simpson, E.L., 1998. Controls on spatial and temporal distribution of Precambrian eolianites. Sediment. Geol. 120, 275–294. doi:10.1016/S0037-0738(98)00036-0

Eriksson, K.A., Simpson, E.L., 2000. Quantifying the oldest tidal record: The 3.2 Ga Moodies Group, Barberton Greenstone Belt, South Africa. Geology 28, 831. doi:10.1130/0091-7613(2000)28<831:QTOTRT>2.0.CO;2

Eriksson, K.A., Simpson, E.L., 2004. Precambrian tidalites: recognition and significance, in: Eriksson, P.G., Altermann, W., Nelson, D.R., Mueller, W.U., Catuneanu, O. (Eds.), The Precambrian Earth: Tempos and Events. Elsevier (Developments in Precambrian Geology), Amsterdam, pp. 631–642.

Eriksson, K.A., Simpson, E.L., Mueller, W.U., 2006. An unusual fluvial to tidal transition in the mesoarchean Moodies Group, South Africa: A response to high tidal range and active tectonics. Sediment. Geol. 190, 13–24. doi:10.1016/j.sedgeo.2006.05.011

Eriksson, P.G., 1999. Sea level changes and the continental freeboard concept: general principles and application to the Precambrian. Precambrian Res. 97, 143–154. doi:10.1016/S0301-9268(99)00029-7

Eriksson, P.G., Bumbb, A.J., Mostert, P., 2004. Early precambrian epeiric seas, in: Eriksson, P.G., Altermann, W., Nelson, D.R., Mueller, W.U., Catuneanu, O. (Eds.), The Precambrian Earth: Tempos and Events. Elsevier (Developments in Precambrian Geology), Amsterdam, pp. 657–660.

Eriksson, P.G., Condie, K.C., Tirsgaard, H., Mueller, W.U., Altermann, W., Miall, a. D., Aspler, L.B., Catuneanu, O., Chiarenzelli, J.R., 1998. Precambrian clastic sedimentation systems. Sediment. Geol. 120, 5–53. doi:10.1016/S0037-0738(98)00026-8

Eriksson, P.G., Porada, H., Banerjee, S., Bouougri, E., Sarkar, S., Bumbb, A.J., 2007. Mat-destruction features, in: Schieber, J., Bose, P.K., Eriksson, P.., Banerjee, S., Sarkar, S., Altermann, W., Catuneanu, O. (Eds.), Atlas of Microbial Mat Features Preserved within the Siliciclastic Rock Record. Elsevier, Amsterdam, pp. 76–105.

Eriksson, P.G., Sarkar, S., Banerjee, S., Porada, H., Catuneanu, O., Samanta, P., 2010. Paleoenvironmental context of microbial mat-related structures in siliciclastic rocks — examples from the Proterozoic of India and South Africa, in: Seckbach, J., Oren, A. (Eds.), Microbial Mats: Modern and Ancient Microorganisms in Stratified Systems. Springer, Berlin, pp. 73–108.

Farquhar, J., Zerkle, A.L., Bekker, A., 2011. Geological constraints on the origin of oxygenic photosynthesis. Photosynth. Res. 107, 11–36. doi:10.1007/s11120-010-9594-0

Flannery, D.T., Walter, M.R., 2011. Archean tufted microbial mats and the Great Oxidation Event: new insights into an ancient problem. Aust. J. Earth Sci. 59, 1–11. doi:10.1080/08120099.2011.607849

Fralick, P., Zaniewski, K., 2012. Sedimentology of a wet, pre-vegetation floodplain assemblage. Sedimentology 59, 1030–1049. doi:10.1111/j.1365-3091.2011.01291.x

Frey, S.E., Gingras, M.K., Dashtgard, S.E., 2009. Experimental Studies of Gas-Escape and Water-Escape Structures: Mechanisms and Morphologies. J. Sediment. Res. 79, 808–816. doi:10.2110/jsr.2009.087

Fryberger, S.G., Schenk, C.J., 1988. Pin stripe lamination: a distinctive feature of modern and ancient eolian sediments. Sediment. Geol. 55, 1–15.

Gamper, A., Heubeck, C., Demskec, D., 2012. Composition and microfacies of Archean microbial mats (Moodies Group, ca. 3.22 Ga, South Africa). Microb. mats siliciclastic … 65–74.

Gerdes, G., 2007. Structures Left by Modern Microbial Mats in Their Host Sediments, in: Schieber, J., Bose, P.K., Eriksson, P.., Banerjee, S., Sarkar, S., Altermann, W., Catuneanu, O. (Eds.), Atlas of Microbial Mat Features Preserved within the Siliciclastic Rock Record. Elsevier, Amsterdam, pp. 5–38. doi:10.1016/S1574-1966(07)02001-9

Gerdes, G., Claes, M., Dunajtschik-Piewak, K., Riege, H., Krumbein, W.E., H.E., R., 1993. Contribution of microbial mats to sedimentary surface structures. Facies 61–74.

Gerdes, G., Klenke, T., Noffke, N., 2000. Microbial signatures in peritidal siliciclastic sediments: a catalogue. Sedimentology 47, 279–308.

Gingras, M.K., 2002. Microbially Induced Sedimentary Structures - A New Category within the Classification of Primary Sedimentary Structures - Discussion. J. Sediment. Res. 72, 587–588.

Grey, K., Hill, A.C., Calver, C., 2011. Biostratigraphy and stratigraphic subdivision of Cryogenian successions of Australia in a global context, in: Arnoud, E., Halverson, G.P., Shields-Zhou, G. (Eds.), The Geological Record of Eoproterozoic Glaciations. Geological Society Memoirs, 36, London, pp. 113–134. doi:10.1144/M36.8

Hall, A.L., 1918. The geology of the Barberton gold mining district. Geol. Surv. South Africa Mem. 1–324.

Heinrichs, T.K., Reimer, T.O., 1977. A sedimentary baryte deposit from the Archean Fig Tree Group of the Barberton Mountain Land (South Africa). Econ. Geol. 72, 1426–1441.

Heubeck, C., 2009. An early ecosystem of Archean tidal microbial mats (Moodies Group, South Africa, ca. 3.2 Ga). Geology 37, 931–934. doi:10.1130/G30101A.1

Heubeck, C., Engelhardt, J., Byerly, G.R., Zeh, A., Sell, B., Luber, T., Lowe, D.R., 2013. Timing of deposition and deformation of the Moodies Group (Barberton Greenstone Belt, South Africa): Very-high-resolution of Archaean surface processes. Precambrian Res. 231, 236–262. doi:10.1016/j.precamres.2013.03.021

Heubeck, C., Lowe, D.R., 1994a. Depositional and tectonic setting of the Archean Moodies Group, Barberton greenstone belt, South Africa. Precambrian Res. 68, 257–290.

Heubeck, C., Lowe, D.R., 1994b. Late syndepositional deformation and detachment tectonics in the Barberton Greenstone Belt, South Africa. Tectonics 13, 1514–1536.

Heubeck, C., Lowe, D.R., 1999. Sedimentary petrography and provenance of the Archean Moodies Grou, Barberton Greenstone Belt, in: Lowe, D.R., Byerly, G.R. (Eds.), Geologic Evolution of the Barberton Greenstone Belt, South Africa. Geological Society of America Special Paper 329, pp. 259–286.

Hofmann, A., 2005. The geochemistry of sedimentary rocks from the Fig Tree Group, Barberton greenstone belt: Implications for tectonic, hydrothermal and surface processes during mid-Archaean times. Precambrian Res. 143, 23–49. doi:10.1016/j.precamres.2005.09.005

Holland, H., 2002. Volcanic gases, black smokers, and the Great Oxidation Event. Geochim. Cosmochim. Acta 66, 3811–3826.

Holland, H.D., 2006. The oxygenation of the atmosphere and oceans. Philos. Trans. R. Soc. Lond. B. Biol. Sci. 361, 903–15. doi:10.1098/rstb.2006.1838

Homann, M., Heubeck, C., Airo, A., Tice, M.M., Nabhan, S., 2013. Microbially-induced carbonate precipitation, Moodies Group (3.2 Ga, BGB, South Africa), in: Mineralogical Magazine. p. 1316. doi:10.1180/minmag.2013.077.5.8

Jahnert, R.J., Collins, L.B., 2012. Characteristics, distribution and morphogenesis of subtidal microbial systems in Shark Bay, Australia. Mar. Geol. 303-306, 115–136. doi:10.1016/j.margeo.2012.02.009

Jahnert, R.J., Collins, L.B., 2013. Controls on microbial activity and tidal flat evolution in Shark Bay, Western Australia. Sedimentology 60, 1071–1099. doi:10.1111/sed.12023

Javaux, E.J., Marshall, C.P., Bekker, A., 2010. Organic-walled microfossils in 3.2-billion-year-old shallow-marine siliciclastic deposits. Nature 463, 934–8. doi:10.1038/nature08793

Johnson, H.D., Baldwin, C.T., 1996. Shallow siliciclastic seas, in: Reading, H.G. (Ed.), Sedimentary Environments; Processes, Facies and Stratigraphy. Blackwell Science, Cambridge, p. 688.

Klausen, M.B., Söderlund, U., Olsson, J.R., Ernst, R.E., Armoogam, M., Mkhize, S.W., Petzer, G., 2010. Petrological discrimination among Precambrian dyke swarms: Eastern Kaapvaal craton (South Africa). Precambrian Res. 183, 501–522. doi:10.1016/j.precamres.2010.01.013

Kreisa, R.D., Moila, R.J., 1986. Sigmoidal tidal bundles and other tidegenerated sedimentary structures of the Curtis Formation. GSA Bull. 97, 381–387.

Krumbein, W.E., Paterson, D.M., Stal, L.J. (Eds.), 1994. Biostabilization of Sediments. BIS, Oldenburg.

Lamb, S., Paris, I., 1988. Post-onverwacht group stratigraphy in the SE part of the Archaean Barbeton greenstone belt. J. African Earth Sci. (and Middle East) 7, 285–306. doi:10.1016/0899-5362(88)90074-7

Layer, P.W., Kroner, A., McWilliams, M., 1996. An Archean Geomagnetic Reversal in the Kaap Valley Pluton, South Africa. Science 273, 943–946.

Long, D.G.F., 2004. Precambrian rivers, in: Eriksson, P.G., Altermann, W., Nelson, D.R., Mueller, W.U., Catuneanu, O. (Eds.), The Precambrian Earth: Tempos and Events. Elsevier (Developments in Precambrian Geology), Amsterdam, pp. 660–663.

Lowe, D.R., 1975. Water escape structures in coarse-grained sediments. Sedimentology 22, 157–204.

Lowe, D.R., Byerly, G.R., 1999. Stratigraphy of the west-central part of the Barberton Greenstone Belt, South Africa, in: Lowe, D.R., Byerly, G.R. (Eds.), Geologic Evolution of the Barberton Greenstone Belt, South Africa. Geological Society of America Special Paper 329, pp. 1–36.

Lowe, D.R., Byerly, G.R., 2007. An overview of the geology of the Barberton Greenstone Belt and vicinity: implications for early crustal development., in: Van Kranendonk, M.J.; Smithies, R.H.; Bennett, V.H. (Ed.), Earth's Oldest Rocks. Elsevier (Developments in Precambrian Geology), Amsterdam, pp. 481–526.

Lowe, D.R., Byerly, G.R., Heubeck, C., 2012. Geologic Map of the west-central Barberton Greenstone Belt, in: South Africa, Scale 1:25,000. Geological Society of America Map and Chart Series No. 103, Boulder. doi:10.1130/2012. MCH103

Lyons, N.A., Kolter, R., 2015. On the evolution of bacterial multicellularity. Curr. Opin. Microbiol. 24, 21–28. doi:10.1016/j.mib.2014.12.007

Lyons, T.W., Reinhard, C.T., Planavsky, N.J., 2014. The rise of oxygen in Earth's early ocean and atmosphere. Nature 506, 307–15. doi:10.1038/nature13068

McCollom, T.M., Seewald, J.S., 2006. Carbon isotope composition of organic compounds produced by abiotic synthesis under hydrothermal conditions. Earth Planet. Sci. Lett. 243, 74–84. doi:10.1016/j.epsl.2006.01.027

Mukhopadhyay, J., Crowley, Q.G., Ghosh, S., Ghosh, G., Chakrabarti, K., Misra, B., Heron, K., Bose, S., 2014. Oxygenation of the Archean atmosphere: New paleosol constraints from eastern India. Geology 42, 923–926. doi:10.1130/G36091.1

Myrow, P.M., 1992. Pot and gutter casts from the Chapel Island Formation, southeast Newfoundland. J. Sediment. Petrol. 62, 992–1007.

Nichols, G., 2009. The Marine Realm: Morphology and Processes, in: Sedimentology and Stratigraphy. Wiley-Blackwell, pp. 163–178.

Noffke, N., 1999. Erosional remnants and pockets evolving from biotic–physical interactions in a Recent lower supratidal environment. Sediment. Geol. 123, 175–181. doi:10.1016/S0037-0738(98)00135-3

Noffke, N., 2010. Microbial Mats in Sandy Deposits from the Archean to Today. Springer, Heidelberg.

Noffke, N., Christian, D., Wacey, D., Hazen, R.M., 2013. Microbially induced sedimentary structures recording an ancient ecosystem in the ca. 3.48 billion-year-old Dresser Formation, Pilbara, Western Australia. Astrobiology 13, 1103–24. doi:10.1089/ast.2013.1030

Noffke, N., Eriksson, K.A., Hazen, R.M., Simpson, E.L., 2006. A new window into Early Archean life: Microbial mats in Earth's oldest siliciclastic tidal deposits (3.2 Ga Moodies Group, South Africa). Geology 34, 253. doi:10.1130/G22246.1

Noffke, N., Gerdes, G., Klenke, T., Krumbein, W., 1997. A microscopic sedimentary succession of graded sand and microbial mats in modem siliciclastic tidal flats. Sediment. Geol. 110, 1–6.

Noffke, N., Gerdes, G., Klenke, T., Krumbein, W., 2001a. Microbially induced sedimentary structures - A new category within the classification of primary sedimentary structures. J. Sediment. Res. 71, 649–656.

Noffke, N., Gerdes, G., Klenke, T., Krumbein, W.E., 2001b. Microbially induced sedimentary structures indicating climatological, hydrological and depositional conditions within Recent and Pleistocene coastal facies zones (Southern Tunesia). Facies 49, 23–30.

Petroff, A.P., Sim, M.S., Maslov, A., Krupenin, M., Rothman, D.H., Bosak, T., 2010. Biophysical basis for the geometry of conical stromatolites. Proc. Natl. Acad. Sci. U. S. A. 107, 9956–61. doi:10.1073/pnas.1001973107

Pflüger, F., Gresse, P.G., 1996. Microbial sand chips- a non-actualistic sedimentary structure. Sediment. Geol. 102, 263–274.

Phoenix, V.R., Konhauser, K.O., Adams, D.G., Bottrell, S.H., 2001. Role of biomineralization as an ultraviolet shield: Implications for Archean life. Geology 29, 823–826. doi:10.1130/0091-7613(2001)029<0823:ROBAAU>2.0.CO

Planavsky, N.J., Asael, D., Hofmann, A., Reinhard, C.T., Lalonde, S.V., Knudsen, A., Wang, X., Ossa Ossa, F., Pecoits, E., Smith, A.J.B., Beukes, N.J., Bekker, A., Johnson, T.M., Konhauser, K.O., Lyons, T.W., Rouxel, O.J., 2014. Evidence for oxygenic photosynthesis half a billion years before the Great Oxidation Event. Nat. Geosci. 7, 283–286. doi:10.1038/ngeo2122

Reid, R.P., Visscher, P.T., Decho, A.W., Stolz, J.F., Bebout, B.M., Dupraz, C., Macintyre, I.G., Paerl, H.W., Pinckney, J.L., Prufert-Bebout, L., Steppe, T.F., DesMarais, D.J., 2000. The

role ofmicrobes in accretion, lamination and early lithication of modern marine stromatolites. Nature 406, 989–992.

Reyes, K., Gonzalez, N.I., Stewart, J., Ospino, F., Nguyen, D., Cho, D.T., Ghahremani, N., Spear, J.R., Johnson, H.A., 2013. Surface orientation affects the direction of cone growth by leptolyngbya sp. Strain C1, a likely architect of coniform structures octopus spring (Yellowstone National Park). Appl. Environ. Microbiol. 79, 1302–1308. doi:10.1128/AEM.03008-12

Sarkar, S., Banerjee, S., 2014. Microbial mat records in siliciclastic rocks: Examples from Four Indian Proterozoic basins and their modern equivalents in Gulf of Cambay. J. Asian Earth … 5.

Schidlowski, M., 2001. Carbon isotopes as biogeochemical recorders of life over 3.8 Ga of Earth history: evolution of a concept. Precambrian Res. 106, 117–134. doi:10.1016/S0301-9268(00)00128-5

Schieber, J., 1999. Microbial Mats in Terrigenous Clastics : The Challenge of Identification in the Rock Record. Palaios 14, 3–12.

Schieber, J., 2004. Microbial mats in the siliciclastic rock record: a summary of diagnostic features, in: Eriksson, P.G., Altermann, W., Nelson, D.R., Mueller, W.U., Catuneanu, O. (Eds.), The Precambrian Earth: Tempos and Events. Elsevier (Developments in Precambrian Geology), Amsterdam, pp. 663–673.

Schieber, J., Bose, P.K., Eriksson, P.G., 2007. Atlas of microbial mat features preserved within the siliciclastic rock record. Elsevier, Amsterdam.

Schirrmeister, B.E., de Vos, J.M., Antonelli, A., Bagheri, H.C., 2013. Evolution of multicellularity coincided with increased diversification of cyanobacteria and the Great Oxidation Event. Proc. Natl. Acad. Sci. U. S. A. 110, 1791–6. doi:10.1073/pnas.1209927110

Schopf, J.. W., 1993. Microfossils of the Early Archean Apex Chert: New Evidence of the Antiquity of Life. S 260, 640–646.

Schopf, J.W., 1977. Biostratigraphic usefulness of stromatolitic Precambrian microbiotas: A preliminary analysis. Precambrian Res. 5, 143–173.

Schopf, J.W., 2004. Geochemical and submicron-scale morphologic analyses of individual Precambrian microorganisms. Geochemical Soc. Spec. Publ. 365–375.

Schopf, J.W., 2006. Fossil evidence of Archaean life. Philos. Trans. R. Soc. Lond. B. Biol. Sci. 361, 869–85. doi:10.1098/rstb.2006.1834

Schopf, J.W., 2011. The paleobiological record of photosynthesis. Photosynth. Res. 107, 87–101. doi:10.1007/s11120-010-9577-1

Schopf, J.W., Kudryavtsev, A.B., 2005. Three-dimensional Raman imagery of precambrian microscopic organisms. Geobiology 1–12.

Schopf, J.W., Kudryavtsev, A.B., 2009. Confocal laser scanning microscopy and Raman imagery of ancient microscopic fossils. Precambrian Res. 173, 39–49. doi:10.1016/j.precamres.2009.02.007

Shepard, R.N., Sumner, D.Y., 2010. Undirected motility of filamentous cyanobacteria produces reticulate mats. Geobiology 8, 179–90. doi:10.1111/j.1472-4669.2010.00235.x

Sim, M.S., Liang, B., A.P., P., Evans, A., Klepac-Ceraj, V., Flannery, D.T., Walter, M.R., 2012. Oxygen-Dependent Morphogenesis of Modern Clumped Photosynthetic Mats and Implications for the Archean Stromatolite Record. Geosciences 2, 235–259. doi:10.3390/geosciences2040235

Simpson, E.L., Eriksson, K.A., Mueller, W.U., 2012. 3.2 Ga eolian deposits from the Moodies Group, Barberton Greenstone Belt, South Africa: Implications for the origin of first-cycle quartz sandstones. Precambrian Res. 214-215, 185–191. doi:10.1016/j.precamres.2012.01.019

Stubblefield, W.L., McGrail, D.W., Kersey, D.G., 1984. Recognition of transgressive and post-transgressive sand ridges on the New Jersey continental shelf, in: Tillman, R.W., Siemers, C.T. (Eds.), Siliciclastic Shelf Sediments. SEPM, Tulsa, pp. 1–23.

Sumner, D.Y., 1997. Late Archean calcite-microbe interactions; two morphologically distinct microbial communities that affected calcite nucleation differently. Palaios 12, 302–318.

Taj, R.J., Aref, M. a. M., Schreiber, B.C., 2014. The influence of microbial mats on the formation of sand volcanoes and mounds in the Red Sea coastal plain, south Jeddah, Saudi Arabia. Sediment. Geol. 311, 60–74. doi:10.1016/j.sedgeo.2014.06.006

Terwindt, J.H.J., 1988. Paleo-tidal reconstructions of inshore tidal depositional environments, in: De Boer, P.L., Van Gelder, A., Nio, S.D. (Eds.), Tide-Influenced Sedimentary Environments and Facies. D. Reidel Publishing Company, Dordrecht, pp. 233–263.

Tice, M.M., 2009. Environmental Controls on Photosynthetic Microbial Mat Distribution and Morphogenesis on a 3.42Ga Clastic-Starved Platform. Astrobiology 9, 989–1000.

Tice, M.M., B.C., B., Lowe, D.R., 2004. Thermal history of the 3.5–3.2 Ga Onverwacht and Fig Tree Groups, Barberton greenstone belt, South Africa, inferred by Raman microspectroscopy of carbonaceous material. Geology 32, 37. doi:10.1130/G19915.1

Tice, M.M., Lowe, D.R., 2006. Hydrogen-based carbon fixation in the earliest known photosynthetic organisms. Geology 34, 37. doi:10.1130/G22012.1

Tice, M.M., Thornton, D.C.O., Pope, M.C., Olszewski, T.D., Gong, J., 2011. Archean Microbial Mat Communities. Annu. Rev. Earth Planet. Sci. 39, 297–319. doi:10.1146/annurev-earth-040809-152356

Toulkeridis, T., Goldstein, S.L., Clauer, N., Kröner, A., Todt, W., Schidlowski, M., 1998. Sm-Nd, Rb-Sr and Pb-Pb dating of silicic carbonates from the early Archaean Barberton Greenstone Belt, South Africa: evidence for post-depositional isotopic resetting at low temperature. Precambrian Res. 92, 129–144.

Trainer, M.G., Pavlov, A.A., Langley DeWitt, H., Jimenez, J.L., McKay, C.P., Toon, O.B., Tolbert, M.A., 2006. Organic haze on Titan and the early Earth. Proc. Natl. Acad. Sci. U. S. A. 18035–42. doi:10.1073/pnas.0608561103

Van Kranendonk, M., Smithies, R.H., Bennett, V.C., 2007. Earth's oldest rocks. Dev. Precambrian Geol. 15.

Viljoen, M.J., Viljoen, R.P., 1969. An introduction to the geology of the Barberton granite-greenstone terrain. Spec. Publ. Geol. Soc. S. Afr 2, 9–28.

Visser, D., 1956. The geology of the Barberton area. Geol. Soc. S. Afr. Spec. Publ. 15, 253.

Wacey, D., 2009. Early Life on Earth. A Practical Guide, Topics in Geobiology , Vol. 31. Springer.

Wacey, D., Gleeson, D., Kilburn, M.R., 2010. Microbialite taphonomy and biogenicity: new insights from NanoSIMS. Geobiology 8, 403–16. doi:10.1111/j.1472-4669.2010.00251.x

Wacey, D., Menon, S., Green, L., Gerstmann, D., Kong, C., McLoughlin, N., Saunders, M., Brasier, M., 2012. Taphonomy of very ancient microfossils from the ~3400Ma Strelley Pool Formation and ~1900Ma Gunflint Formation: New insights using a focused ion beam. Precambrian Res. 220-221, 234–250. doi:10.1016/j.precamres.2012.08.005

Wacey, D., Saunders, M., Roberts, M., Menon, S., Green, L., Kong, C., Culwick, T., Strother, P., Brasier, M.D., 2014. Enhanced cellular preservation by clay minerals in 1 billion-year-old lakes. Sci. Rep. 4, 5841. doi:10.1038/srep05841

Walsh, M.M., 1992. Microfossils and possible microfossils from the Early Archean Onverwacht Group, Barberton Mountain Land, South Africa. Precambrian Res. 54, 271–293.

Walsh, M.M., Lowe, D.R., 1985. Filamentous microfossils from the 3,500-Myr-old Onverwacht Group, Barberton Mountain Land, South Africa. Nature 314, 530–531.

Walsh, M.M., Lowe, D.R., 1999. Modes of accumulation of carbonaceous matter in the Early Archean: a petrographic and geochemical study of the carbonaceous cherts of the

Swaziland Supergroup, in: Lowe, D.R., Byerly, G.R. (Eds.), Geologic Evolution of the Barberton Greenstone Belt, South Africa. Geological Society of America Special Paper 329, pp. 115–132.

Walsh, M.M., Westall, F., 2003. Archean biofilms preserved in the Swaziland Supergroup, South Africa, in: Krumbein, W.E., Paterson, D.M., Zavarzin, G.A. (Eds.), Fossil and Recent Biofilms: A Natural History of Life on Earth. Kluwer, Dordrecht, pp. 307–316.

Walter, M.R., Bauld, J., Brock, T.D., 1976. Microbiology and morphogenesis of columnar stromatolites (Conophyton, Vacerrila) from hot springs in Yellowstone National Park, in: Walter, M.R. (Ed.), Stromatolites. Elsevier, New York, pp. 273–310.

Wells, M.L., 1998. Marine colloids: A neglected dimension. Nature 391, 530–531.

Westall, F., De Ronde, C.E.J., Southam, G., Grassineau, N., Colas, M., Cockell, C., Lammer, H., 2006. Implications of a 3.472-3.333 Gyr-old subaerial microbial mat from the Barberton greenstone belt, South Africa for the UV environmental conditions on the early Earth. Philos. Trans. R. Soc. Lond. B. Biol. Sci. 361, 1857–75. doi:10.1098/rstb.2006.1896

Williams, R.M.E., Grotzinger, J.P., Dietrich, W.E., Gupta, S., Sumner, D.Y., Wiens, R.C., Mangold, N., Malin, M.C., Edgett, K.S., Maurice, S., Forni, O., Gasnault, O., Ollila, A., Newsom, H.E., Dromart, G., Palucis, M.C., Yingst, R. a, Anderson, R.B., Herkenhoff, K.E., Le Mouélic, S., Goetz, W., Madsen, M.B., Koefoed, A., Jensen, J.K., Bridges, J.C., Schwenzer, S.P., Lewis, K.W., Stack, K.M., Rubin, D., Kah, L.C., Bell, J.F., Farmer, J.D., Sullivan, R., Van Beek, T., Blaney, D.L., Pariser, O., Deen, R.G., 2013. Martian fluvial conglomerates at Gale crater. Science (80-.). 340, 1068–72. doi:10.1126/science.1237317

Figures

Fig. 1. Simplified geological map of the Barberton Greenstone Belt (BGB) of South Africa and Swaziland, comprising the Onverwacht, Fig Tree and Moodies groups, in the eastern part of the Kaapvaal Craton. Moodies strata crop out in five synclines north of the Inyoka Fault: the

Stolzburg Syncline, the Moodies Hills Block, the Eureka Syncline, the Dycedale Syncline and the Saddleback Syncline as well as in synclines to the South of the Inyoka Fault. The boxed area shows the study area in the Saddleback Syncline.

Fig. 2. Generalized stratigraphy of the Moodies Group in the Saddleback Syncline in the central BGB. Note that microbial mats in the studied interval are clearly restricted to peritidal, shallow-water paleoenvironments. Stratigraphic abbreviations follow Anhaeusser (1976) and Lowe et al. (2012); MdB = Moodies basal conglomerate, MdQ1 = Moodies medium- to coarse-grained quarzitic sandstone, MdS1 = Moodies fine-grained sand- and siltstones, MdCh = Moodies sandstone with cherty lithic grains, MdQ2 = Moodies coarse-grained quartz arenite. For explanation of symbols and signatures in the column, see legend of Fig. 3.

Fig. 3. Integrated stratigraphic and depositional facies correlation of measured sections in the Saddleback Syncline. Locations of each section are indicated in the topographic map (inset). Microbial mats and related structures (highlighted in green) appear confined to the coastal floodplain, supra- and intertidal paleoenvironments and are absent in the subtidal zone. Note the interval with giant gas-/fluid-escape structures that spans over 7 km in the upper parts of the studied succession in the upper inter- to supratidal facies. Paleoflow is mainly bidirectional and oriented towards the NE and SW in the intertidal and coastal floodplain facies; it appears unidirectional towards the NE in the subtidal facies. For a detailed description of the lithofacies, see Table 1.

Fig. 4. Field photographs of sedimentary structures from the braided fluvial-alluvial (A), coastal floodplain (B and C), upper inter- to supratidal (D and E), and intertidal facies (F - H) in the lower half of the Saddleback Syncline stratigraphy. (A) Cross-section view of polymict, clast-supported conglomerate from the basal Moodies Group. (B) Cross-section view of erosive pebble-cobble bed (in dashed lines). (C) Cross-section view of erosional channel filled with trough-cross-bedded sandstone and lag deposit at the base (arrow). (D) Cross-section view of subhorizontally-laminated sandstone with fenestral fabric. (E) Desiccation cracks on thin mudstone partings filled with coarse-grained sandstone (bedding plane view). (F) Cross-section view of a sigmoidal-shaped foreset and simplified sketch. (G) Bidirectionally-oriented foresets interpreted as herring bone cross stratification. (H) Cross-section view of planar foresets with mud drapes (arrows).

Fig. 5. Field photographs of common sedimentary structures in the subtidal sand ridge deposits. (A) Low angle planar foresets showing almost 4 m of preserved thickness. (B) Bedding plane view of asymmetrical ripples. (C) Cross-section view of straight-crested, symmetrical ripples (arrow). (D) Erosional depression in cross-section view, interpreted as gutter cast.

Fig. 6. (A) Photograph of polished slab (cross-section view) containing abundant remnants of microbial mats (dark wavy laminae) which coat sand ripples, foresets, form small domes and

shrinkage cracks. (B) Transmitted light photomicrograph (of boxed area in A) showing that detrital sand particles are commonly fine- to medium-grained (f-m) below a lamina, fine-grained (f) within and medium-to-coarse-grained (m-c) above a lamina. (C) Close-up view of undulatory kerogenous laminae with fine-grained-sand and silt-sized particles. (D) Trans-X-Ray elemental maps of Ti (purple) and Zr (cyan) show the preferential enrichment of zircon and rutile or anatase in the dark microbial laminae.

Fig. 7. Photographs of polished sandstone slabs (cross-section view) and corresponding sketches, highlighting the mat morphotypes of each paleoenvironment. Reconstructed mat morphologies are indicated in the simplified sketch (top right) for each facies. (A) Planar mats that cover former sedimentary surfaces and occasionally onlap and drape pebbly conglomerate layers; dc = desiccation cracks. (B) Wavy-crinkly mats and small microbial domes (arrow), commonly underlain by bedding-plane-parallel layers of chert. Note that the upper contact of these layers is straight or gently undulating, whereas the lower part is commonly more irregular. (C) Tufted microbial mats with vertically stacked cones that are partially filled with chert and supported by draping laminae (arrows). The successive growth stages of the tufts are depicted by different shades of green.

Fig. 8. Photographs of polished slabs of microbial tufts and domes and comparison with modern analog. (A) Cross-section view of microbial domes that preferentially develop on small topographic highs and may represent initial growth stages of tufts. (B) Cross-section view of a microbial mat showing closely spaced tufts, interconnected by draping laminae

(arrows). The tufts are internally partly filled by chert. (C) Cross-section view of tufted microbial mat from Bahar Alouane (Tunisia) built by vertically oriented bundles of filamentous cyanobacteria. These mats commonly show polygonal patterns of reticulate ridges (arrow) with tufts at ridge junctions in plan view. (D) Cross-section view of two single tufts laterally linked by microbial lamina (arrow). (E) Horizontal section through a tuft layer reveals their sub-circular structure. (F) Transmitted light photomicrograph of a silicified microbial tuft (arrow) with trapped fine-grained sediment. Note the chert-filled void in the central part of the tuft.

Fig. 9. Morphological similarities of gas bubbles trapped in modern tuft from Bahar Alouane, Tunisia in comparison with fossil microbial tuft of the Moodies Group. (A) Polished slab photograph of a tuft with chert-filled void in the central part interpreted as former gas bubble (arrow). (B) Modern tuft with trapped oxygen-rich bubbles enmeshed by filamentous cyanobacteria.

Fig. 10. Field and polished slab photographs of cohesive microbial mats from inter- to supratidal paleoenvironments that experienced periods of subaerial exposure, dehydration, erosion and redeposition. (A) Bedding plane view of a microbial mat-covered surface (mm) with shrinkage cracks exhibiting a polygonal pattern (arrows). Microbial mat chips (mc) are visible adjacent to these cracks. Note that shrinkage cracks are associated with – but distinct from – desiccation-cracked bedding planes. (B) Cross-section view of microbial-mat-bearing sandstone (mm) intersected by a prominent horizon of desiccation-cracked mudstones. (C)

Bedding plane view of microbial mats (mm) associated with microbial mat chips (mc) that presumably were eroded from the edges of the mat (dotted arrows). (D) Eroded mat fragments forming a microbial-sand-chip conglomerate. Note the slightly curved ends of some of the chips (arrows). (E) Cross-section view of densely laminated microbial mats with eroded mat chips (mc) above that presumably had a rigid, cohesive consistency.

Fig. 11. Field photographs of structures related to gas or fluid escape in densely microbial mat-laminated sandstone of the supratidal facies. (A) Cross-section view and simplified sketch of a vertical-oriented gas- or fluid-escape structure bordered by upward-curved microbial mats. The central channel shows a high concentration of carbonaceous material that was probably concentrated in the waning flow. Note the domed mat in the upper part (arrow). (B) Linear cracks on mat-covered bedding plane that may form part of a larger polygonal crack networks. (C) Ruptured gas dome with central depression on a well-preserved bedding plane.

Fig. 12. Transmitted light photomicrographs of chert layers underlying microbial mats in cross-section. (A) Microbial mat (mm) underlain by bedding-plane-parallel, up to 4 mm thick chert layer with patchy remnants of carbonates. (B) Close-up view of the boxed area in A, documenting the partial replacement of carbonate by chert. Note small carbonate remnants within chert (arrow). (C) Close-up view of the boxed area in B, showing corroded and undulatory grain boundaries (arrow), and truncation of dolomite twin lamellae, as well as several nucleation centers of chert.

Fig. S1 Cumulative grain size frequency plot of detrital grains below (blue), within (green), and above a microbial mat (red) and corresponding thin section. (A) The grain size distribution of the three measured areas shows that particles are fine- to medium-grained below, fine-grained within, and medium- to coarse-grained above the mat. Sorting is less in the grains overlying the mat. (B) Transmitted light photomicrograph of the analyzed sandstone sample in cross section view with calculated current velocities. The remains of a former microbial mat (mm) are visible in the central part. Colors correspond to the cumulative frequency curves.

Fig. S2 Polished slab photograph of microbial mats (dark laminae) in cross-section view. Mats are vertically disrupted by a gas- or fluid-escape structure (arrows). Note that the mats are bent upwards and partly dragged into the subvertical linear channel.

Table 1
Facies description and interpretation of the studied succession in the Saddleback Syncline.

	Lithofacies	Lithologic description	Microbial-mat-related structures	Depositional environment	Water depth
1	basal conglomerate	polymict pebble-cobble conglomerate, clast supported interbedded with gravelly sandstone	not observed	braided fluvial to alluvial (Eriksson, 1978, 1980; Heubeck and Lowe, 1994a)	0 - 1 m
2	poorly-sorted, medium- to coarse-grained sandstone with gravel beds	planar and trough cross bedding (up to 0.3 m); gravelly beds extend ~150 m along strike local erosive channels (50 cm-wide) common desiccation cracks	planar microbial laminae pebble-cobble overgrowth rare chert layers, mat chips gas-/fluid-escape structures (~0.2 m)	coastal floodplain paleoflow direction mainly to the NE or SW	0 - 2 m
3	medium-sorted, medium- to coarse-grained sandstone and minor mudstone	horizontal bedding abundant desiccation cracks	microbial mats with tufts (0.3 - 1 cm, when vertically stacked up to 2 cm), filled with nodular chert concretions common chert layers mat chips, shrinkage cracks large gas-/fluid-escape structures (0.5 - 6 m in height), polygonal cracks gas domes, fenestral fabric	upper inter- to supratidal	0 - 3 m
4	medium-sorted, medium- to coarse-grained sandstone with pebble beds	herringbone cross bedding, sigmoidal foreset bundles (up to 0.5 m), mud drapes reactivation surfaces rare desiccation cracks sinuous-crested ripples small channels (10 - 20 cm wide) pebbly conglomerate stringers	wavy-crinkly microbial laminae with small microbial domes abundant chert layers and mat chips gas-/fluid-escape structures (~0.4 m)	intertidal bidirectional paleoflow towards the NE and SW	0 - 5 m
5	well-sorted, large-scale, low-angle, planar foresets (up to 4 m); rare trough cross bedding (20 - 40 cm) straight-crested ripples; gutter casts	not observed	subtidal unidirectional paleoflow to the NE and E	5 - 15 m	
	medium-grained, intensely silicified sandstone				

Table 1
Facies description and interpretation of the studied succession in the Saddleback Syncline.

	Lithofacies	Lithologic description	Microbial-mat-related structures	Depositional environment	Water depth
1	basal conglomerate	polymict pebble-cobble conglomerate, clast supported interbedded with gravelly sandstone	not observed	braided fluvial to alluvial (Eriksson, 1978, 1980; Heubeck and Lowe, 1994a)	0 - 1 m
2	poorly-sorted, medium- to coarse-grained sandstone with gravel beds	planar and trough cross bedding (up to 0.3 m); gravelly beds extend ~150 m along strike local erosive channels (50 cm-wide) common desiccation cracks	planar microbial laminae pebble-cobble overgrowth rare chert layers, mat chips gas-/fluid-escape structures (~0.2 m)	coastal floodplain paleoflow direction mainly to the NE or SW	0 - 2 m
3	medium-sorted, medium- to coarse-grained sandstone and minor mudstone	horizontal bedding abundant desiccation cracks	microbial mats with tufts (0.3 - 1 cm, when vertically stacked up to 2 cm), filled with nodular chert concretions common chert layers mat chips, shrinkage cracks large gas-/fluid-escape structures (0.5 - 6 m in height), polygonal cracks gas domes, fenestral fabric	upper inter- to supratidal	0 - 3 m
4	medium-sorted, medium- to coarse-grained sandstone with pebble beds	herringbone cross bedding, sigmoidal foreset bundles (up to 0.5 m), mud drapes reactivation surfaces rare desiccation cracks sinuous-crested ripples small channels (10 - 20 cm wide) pebbly conglomerate stringers	wavy-crinkly microbial laminae with small microbial domes abundant chert layers and mat chips gas-/fluid-escape structures (~0.4 m)	intertidal bidirectional paleoflow towards the NE and SW	0 - 5 m
5	well-sorted, medium-grained, intensely silicified sandstone	large-scale, low-angle, planar foresets (up to 4 m); rare trough cross bedding (20 - 40 cm) straight-crested ripples; gutter casts	not observed	subtidal unidirectional paleoflow to the NE and E	5 - 15 m

graphical abstract

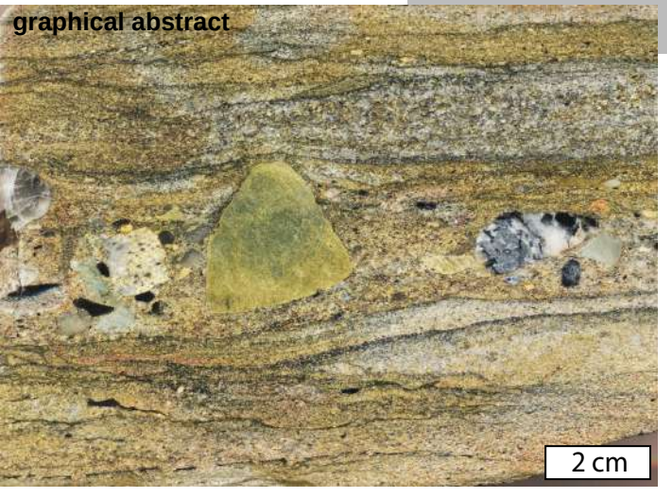

Coastal floodplain

- planar mats

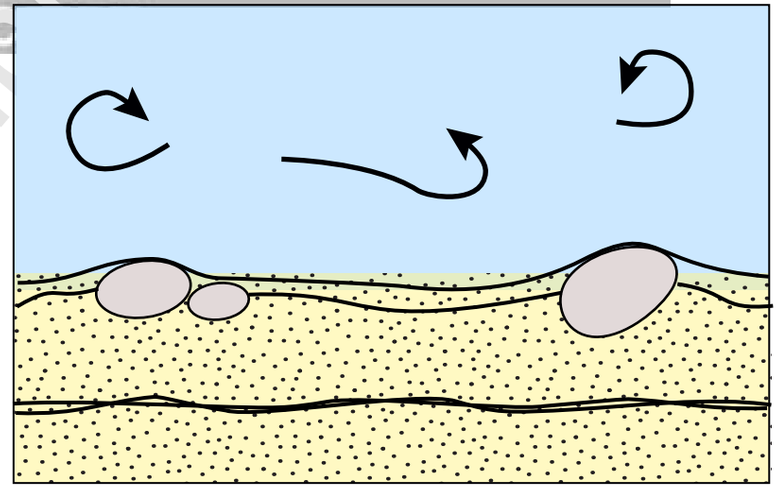

Intertidal

- wavy-crinkly mats with domes

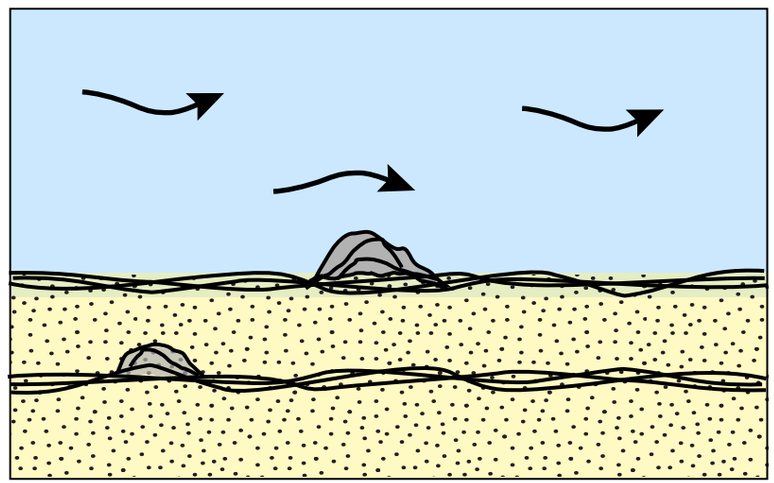

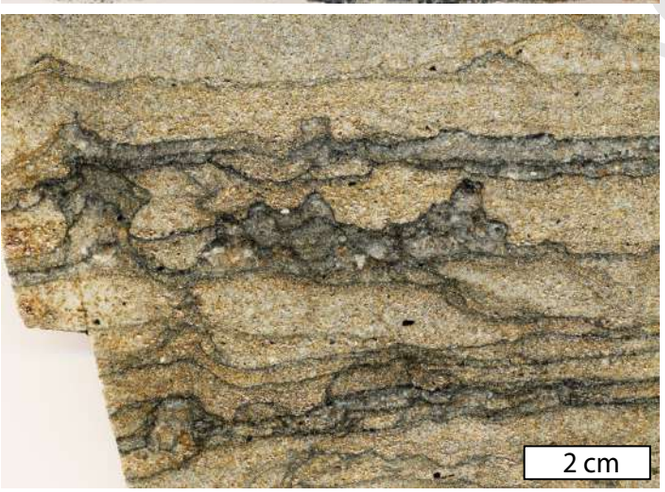

Upper inter- to supratidal

- tufted mats

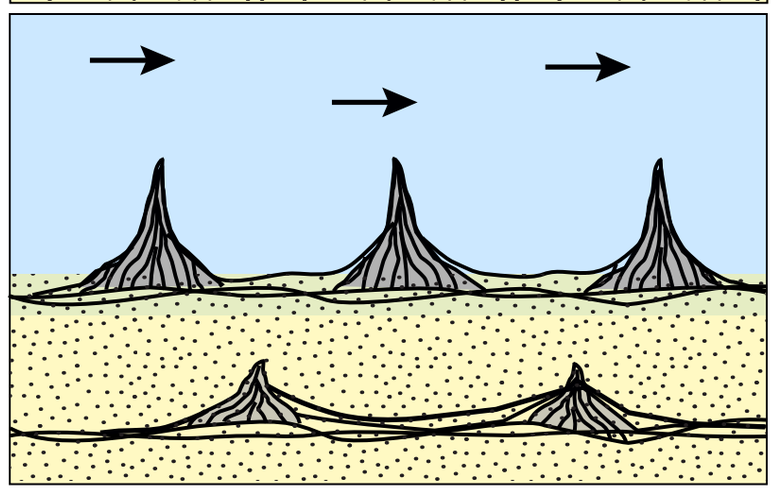

Fig.1 (9cm width)

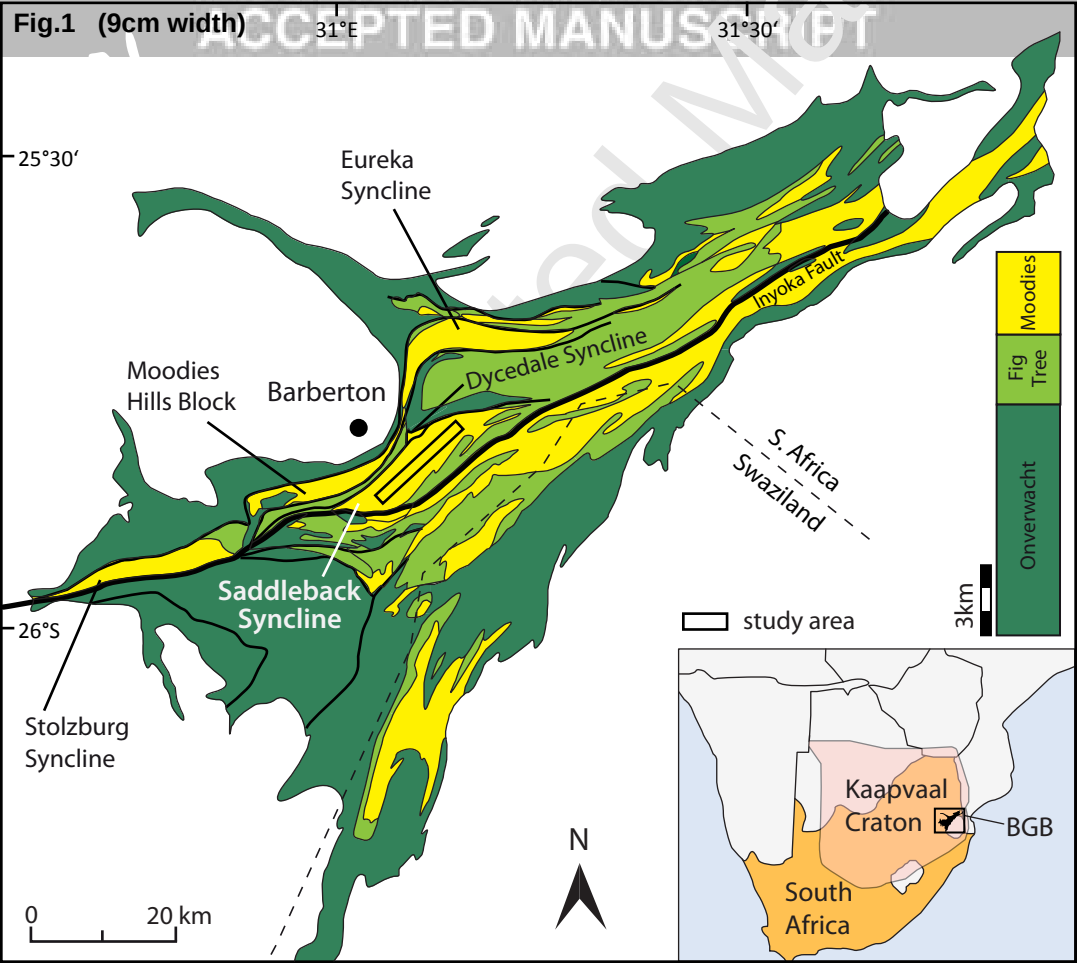

Fig.2 (7 cm width)

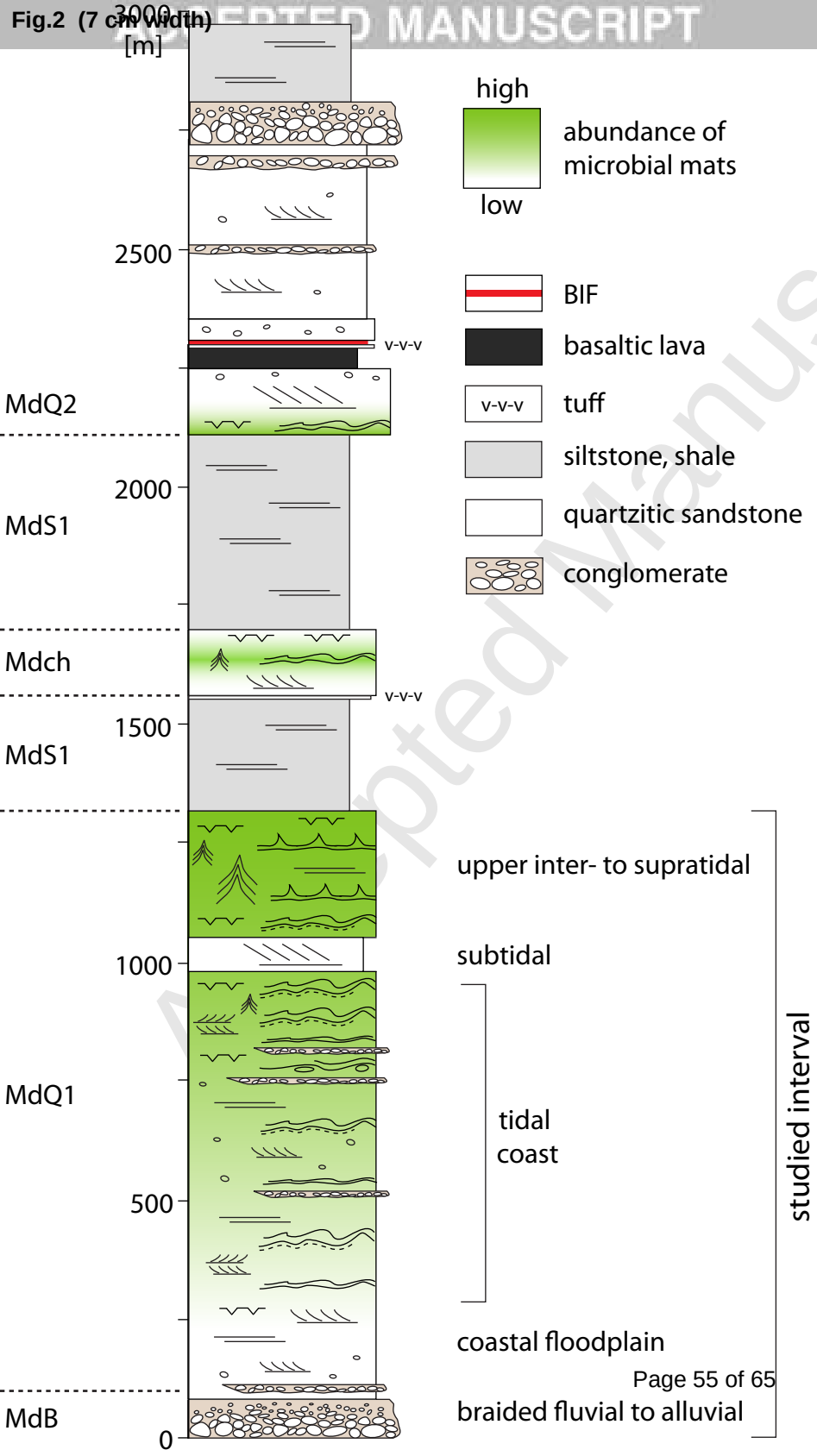

15 km

~1690 m

~200 m

1315 m

1035 m

770 m

520 m

350 m

0 m

905 m

560 m

120 m

0 m

datum

ABUNDANCE OF MICROBIAL MATS

giant gas-/fluid-escape structures

first occurrence of microbial mats

top of basal conglomerate

not exposed

F

?

Saddleback Syncline

Inyoka fault

1800m

1400m

1200m

1500m

SW

NE

1 km

16 17 18 1 2 3 4 5 6 7 8 9 10 11 12 13 14 15

fmc g

n=18 n=22 n=17 n=25 n=9 n=18 n=21 n=25 n=7 n=24 n=17 n=20 n=13 n=6 n=21 n=3 n=15 n=24 n=9

Microbial-mat-related structures

- laminae, flat
- laminae, wavy-crinkly
- laminae, tufted
- mats onlap and overgrow clasts
- mats underlain by chert layers
- microbial-mat chips
- gas-/fluid-escape structures

Facies

- subtidal
- intertidal
- upper inter- to supratidal
- coastal floodplain
- braided fluvial to alluvial

Sedimentary structures

- horizontal lamination
- cross bedding, planar
- cross bedding, trough
- cross bedding, herringbone
- wave-ripple lamination
- desiccation cracks
- gutter casts
- mud layers
- pebbles
- channel
- pebble stringer
- cobble stringer
- paleocurrent rose diagram

Fig.4 (14cm width)

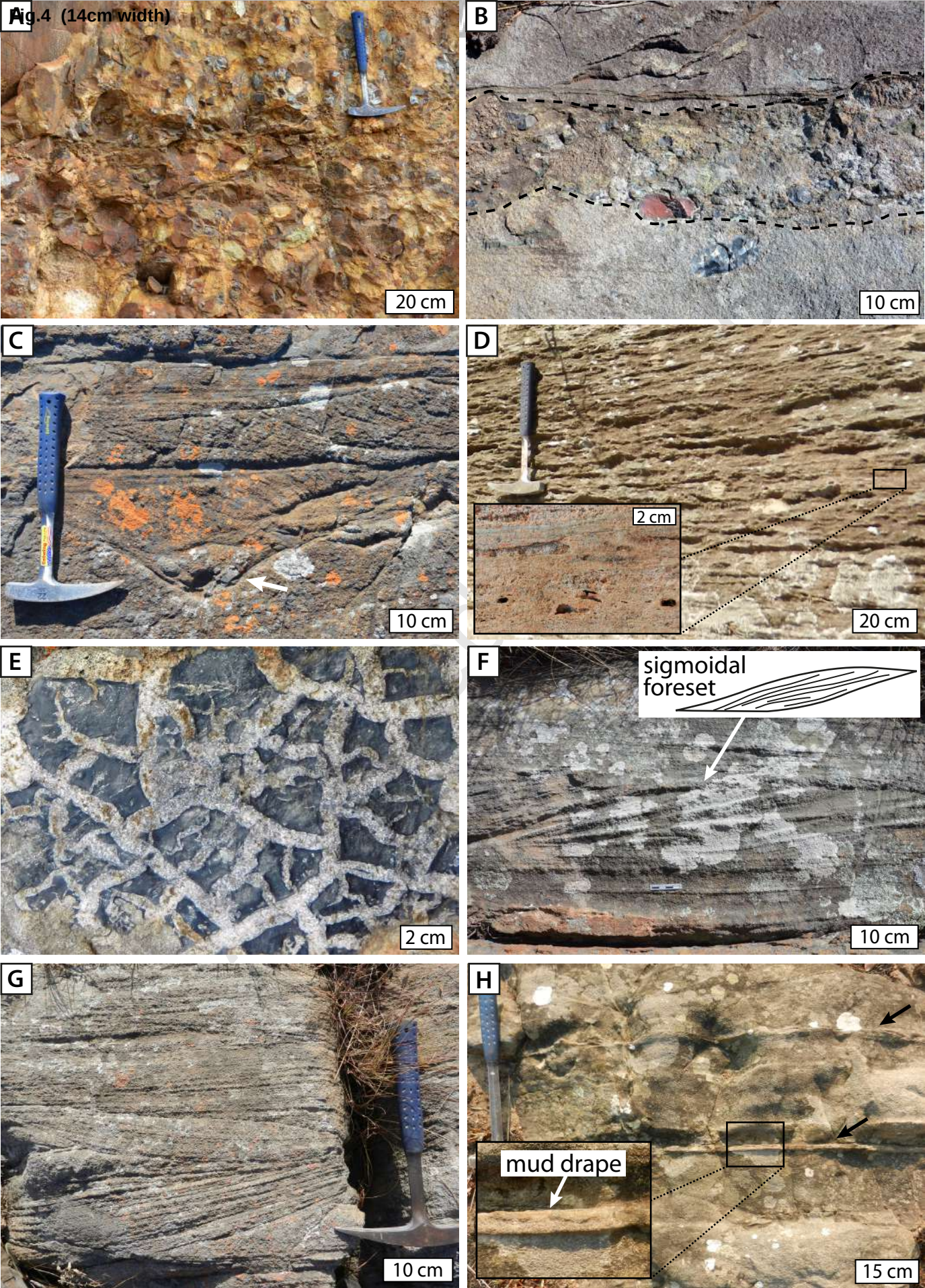

Fig.5 (14cm width)

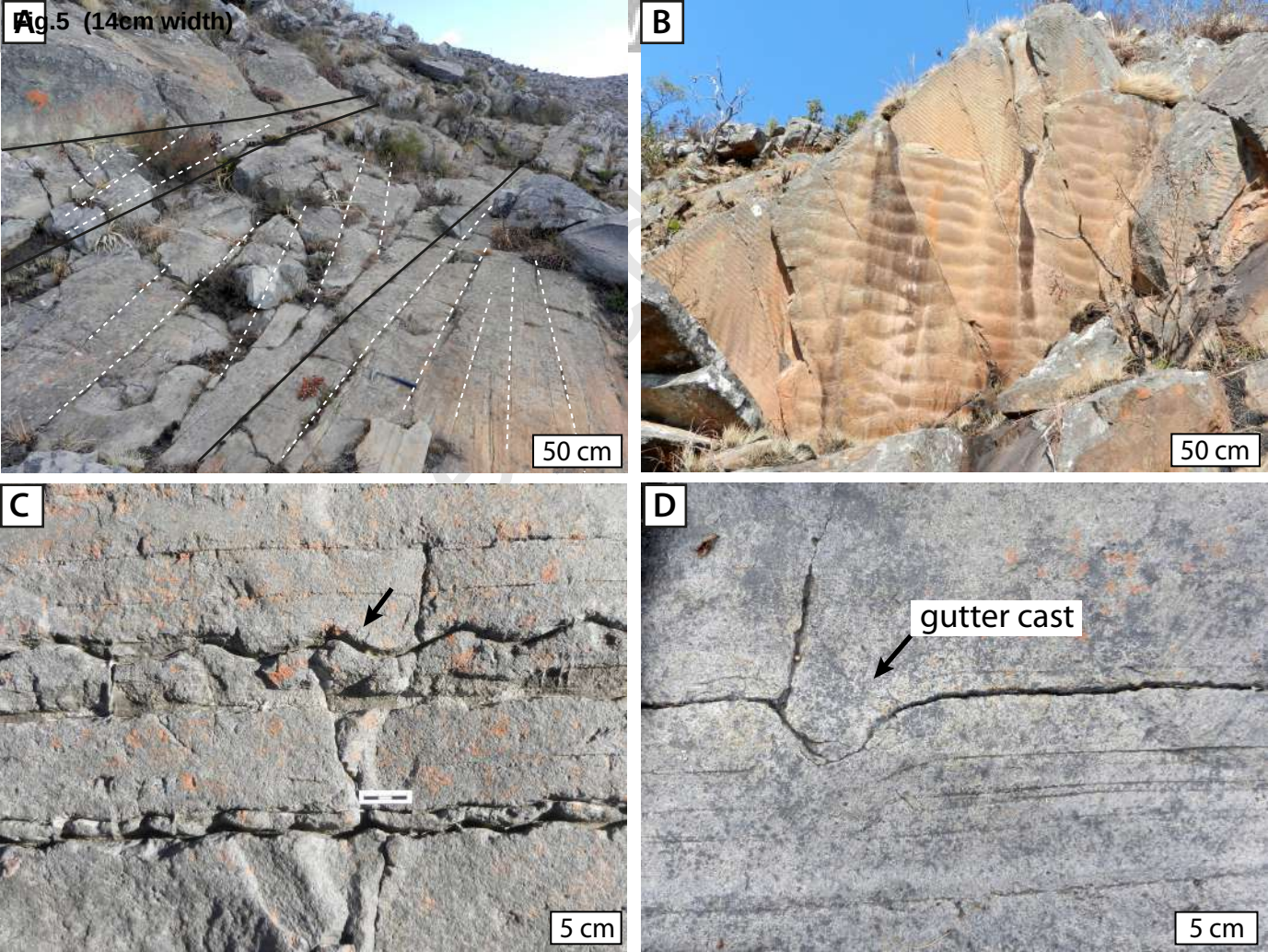

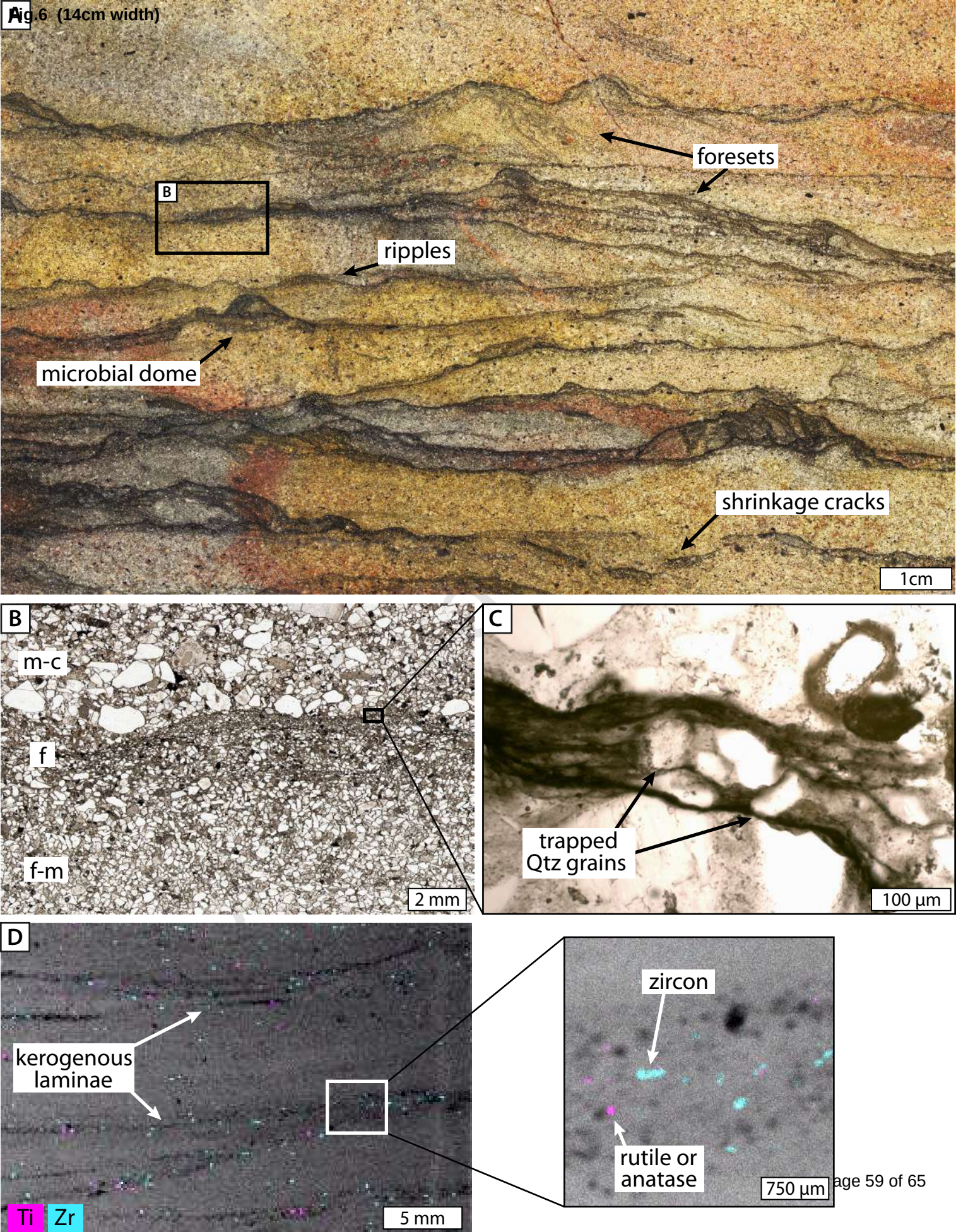
A
B
foresets
ripples
microbial dome
shrinkage cracks
1cm
B
m-c
f
f-m
2 mm
C
trapped
Qtz grains
100 µm
D
kerogenous
laminae
Ti
Zr
5 mm
zircon
rutile or
anatase
750 µm

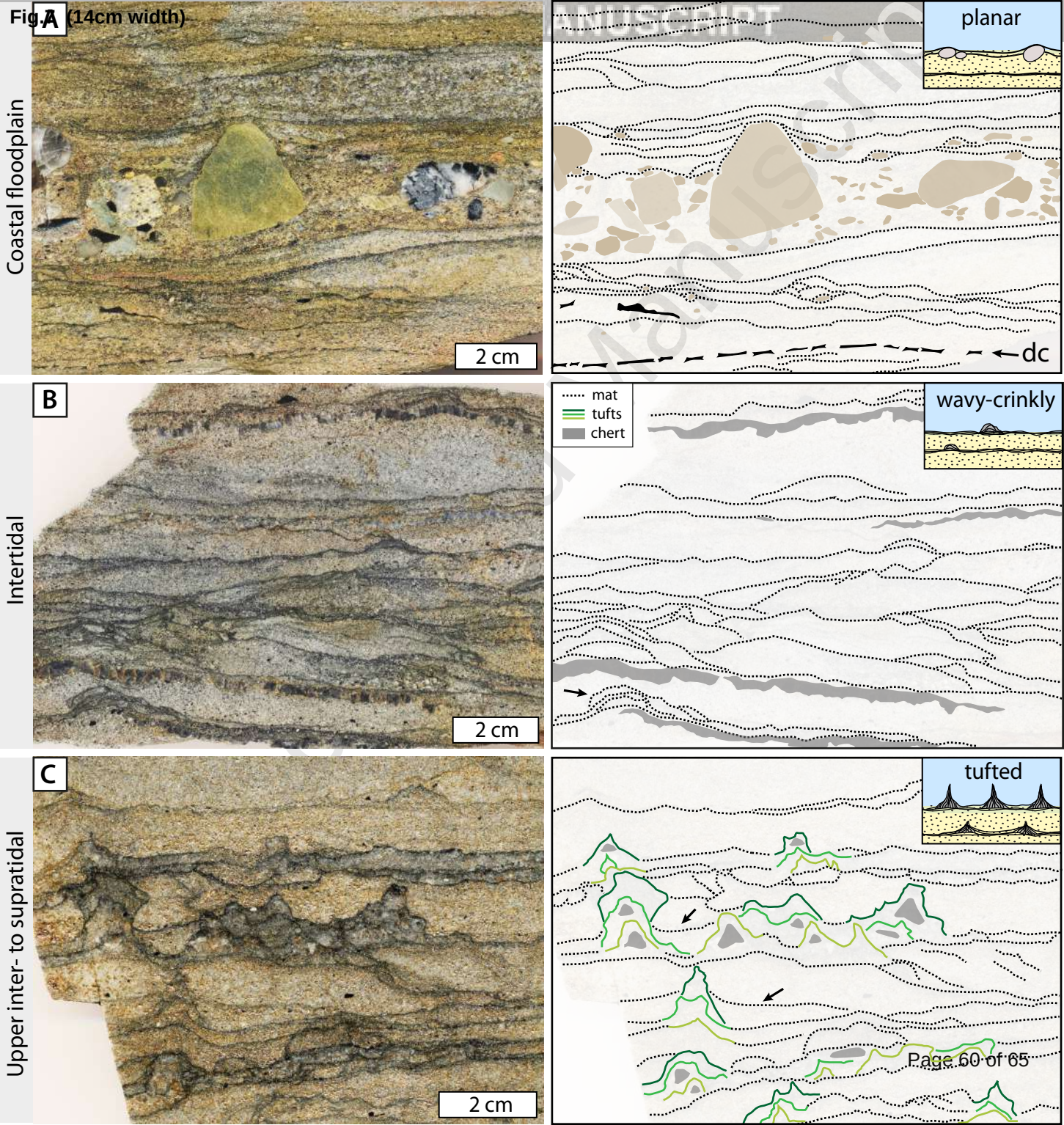
A
Coastal floodplain
2 cm
planar
dc
B
Intertidal
2 cm
mat
tufts
chert
wavy-crinkly
C
Upper inter- to supratidal
2 cm
tufted

Fig.8 (14cm width)

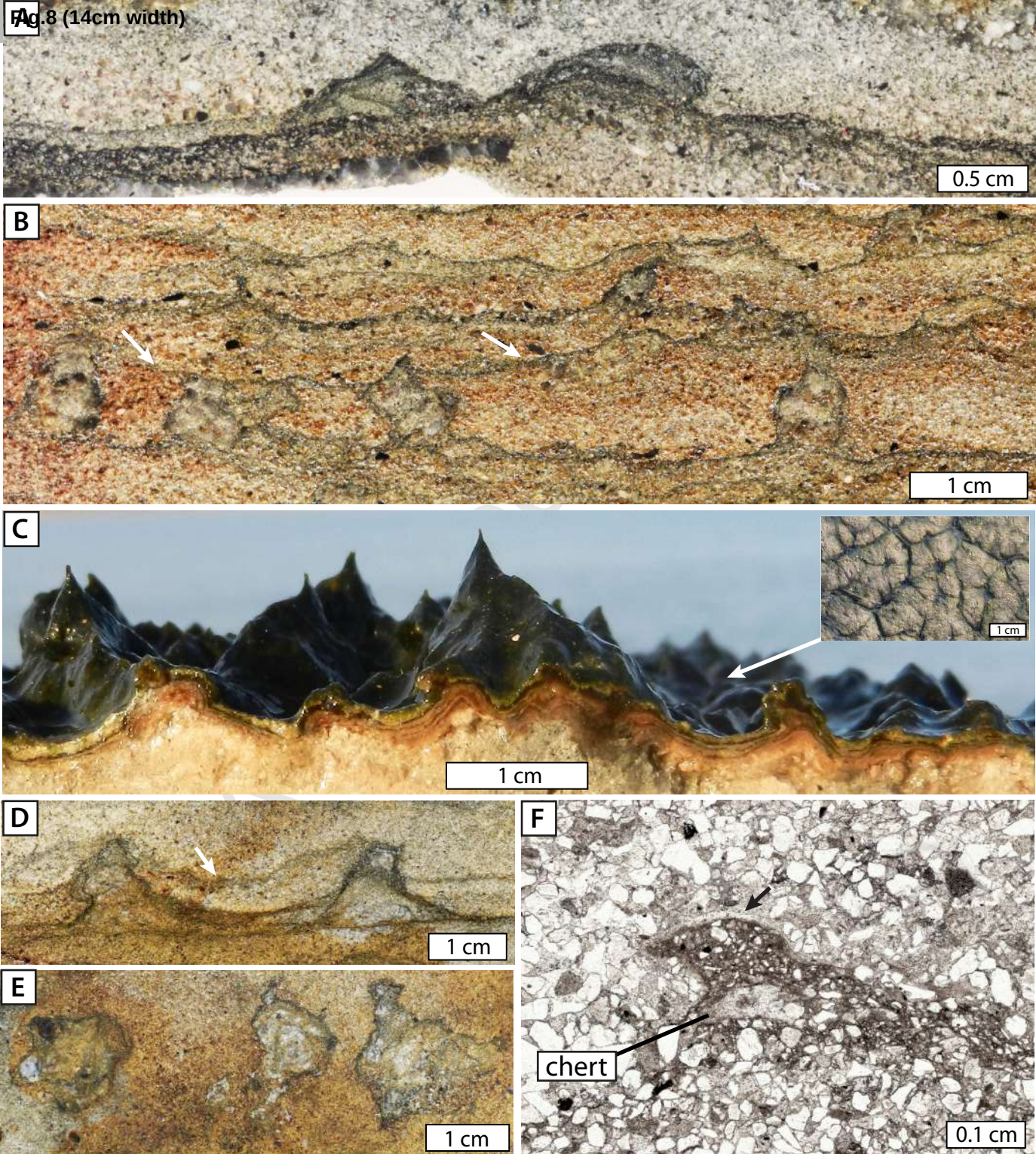

Fig.9 (14cm width)

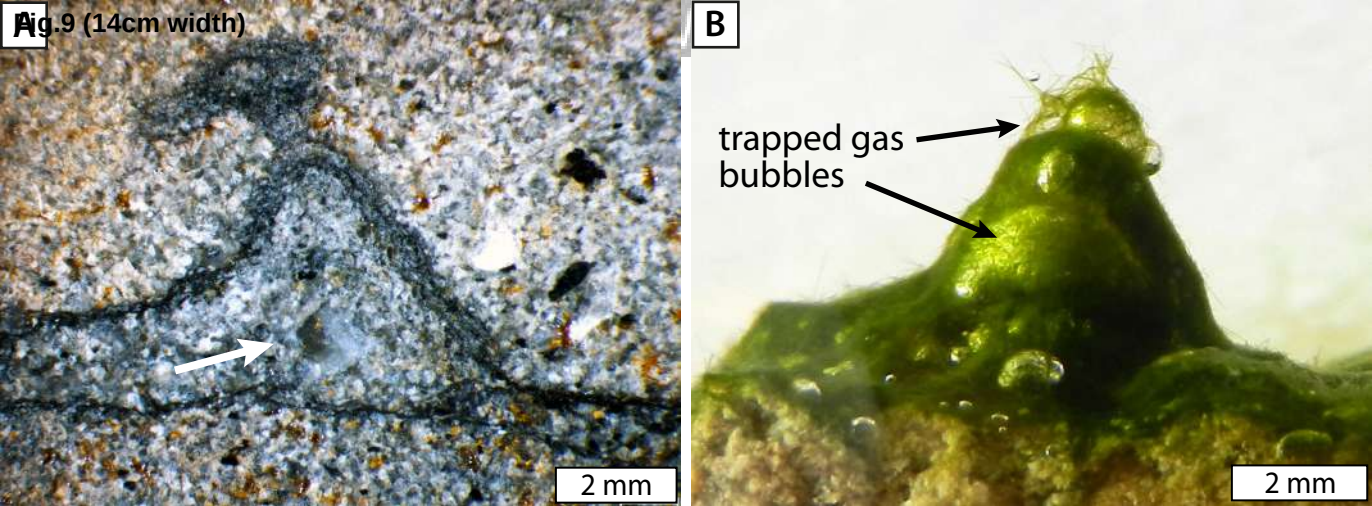

Fig.10 (14cm width)

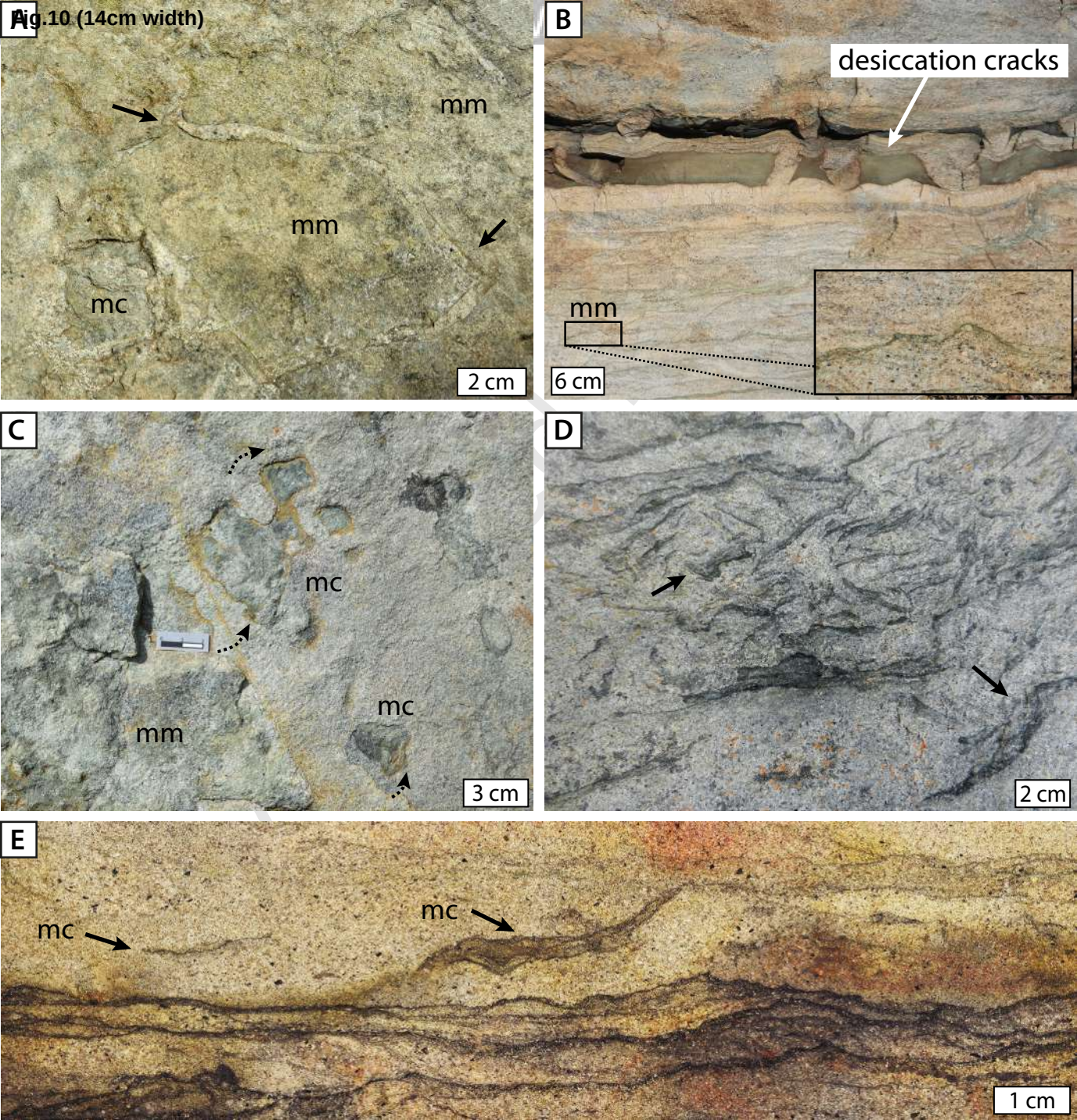

Fig.11 (14cm width)

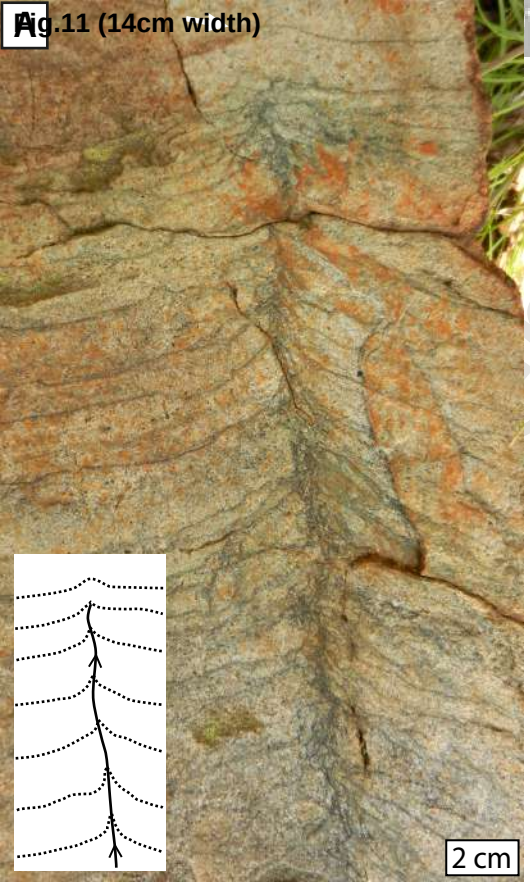

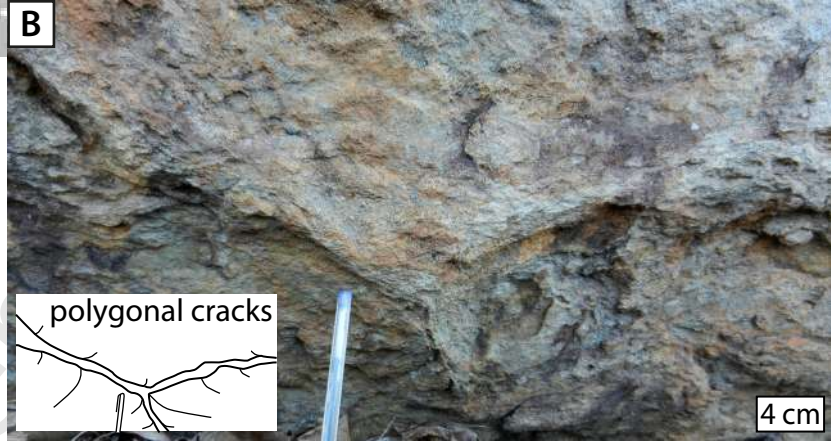

Fig.12 (14cm width)